Research Square

Preprints are preliminary reports that have not undergone peer review.
They should not be considered conclusive, used to inform clinical practice,
or referenced by the media as validated information.

Energy-Efficient Atmospheric Water Harvesting Using MOF-801 and Microwave-Synthesized Al-Fumarate: Linking Micro–Mesoporous Structure to Sorption and Regeneration Behavior

Ayda Naghavi
University of Guilan
fereshteh raouf
f.raouf@guilan.ac.ir
University of Guilan https://orcid.org/0000-0002-4964-251X
Reza Ghasemzadeh
University of Guilan

Research Article

Keywords: Atmospheric Water Harvesting, Micropore, Mesoporous, Water Uptake, Regeneration Energy

Posted Date: June 23rd, 2026

DOI: https://doi.org/10.21203/rs.3.rs-9588362/v1

License: This work is licensed under a Creative Commons Attribution 4.0 International License.
Read Full License

Energy-Efficient Atmospheric Water Harvesting Using MOF-801 and Microwave-Synthesized Al-Fumarate: Linking Micro–Mesoporous Structure to Sorption and Regeneration Behavior

Ayda Naghavi [1], Fereshteh Raouf[1,*], Reza Ghasemzadeh[1]

[1] *Chemical Engineering Department, University of Guilan, Rasht, IRAN, Islamic Republic*

Corresponding Author Email: f.raouf@guilan.ac.ir

Abstract

Atmospheric water harvesting (AWH) has emerged as a promising route to mitigate freshwater scarcity in arid and semi-arid regions. Existing studies typically evaluate individual metal–organic frameworks (MOFs) under limited conditions, leaving a gap in comparative assessments that link pore architecture to sorption behavior. This work aims to establish a direct, climate-relevant comparison between MOF-801 and Al-fumarate, for AWH applications. The sorbents were synthesized and characterized using XRD, FTIR, BET, SEM, and TGA to elucidate their structural and textural properties. Water vapor adsorption–desorption performance was quantified under controlled relative humidity and temperature, supported by thermodynamic analysis of the isosteric heat of adsorption. MOF-801 demonstrated higher water uptake at moderate humidity (0.247 g H_2O g^{-1} at 40% RH and 20 °C), while Al-fumarate showed enhanced performance under more humid conditions (0.278 g H_2O g^{-1} at 80% RH and 25 °C). Both sorbents were regenerated at ~80 °C, corresponding to an energy requirement of 1.2-1.5 MJ L^{-1}. Thermodynamic analysis indicated a higher initial isosteric heat of adsorption (Q_{st}) for MOF-801, consistent with stronger water-framework interactions in drier atmospheres, whereas Al-fumarate exhibited a flatter Q_{st} profile favorable for humid conditions. Both materials were further evaluated in four-month field tests in contrasting humid (Rasht) and arid (Isfahan) climates to assess cycling stability. The results providing practical guidelines for selecting energy-efficient MOFs tailored to specific climatic conditions

Keywords: Atmospheric Water Harvesting; Micropore; Mesoporous; Water Uptake; Regeneration Energy

1. Introduction

The escalating scarcity of freshwater has emerged as one of the most pressing sustainability challenges of the twenty-first century, particularly in arid and semi-arid regions (Xu and Yaghi 2020, Esmaeilion, Ahmadi et al. 2021). Although the Earth contains vast water reserves, over 97% is saline and only about 1% of the total freshwater is easily accessible for human consumption, confined mainly to lakes, rivers, and shallow aquifers. As a result, more than 2.8 billion people are projected to live in water-stressed areas in the near future (Pimentel, Berger et al. 2004, Zhao, Li et al. 2020, Tashtoush and Alshoubaki 2023). Iran's ongoing water crisis driven by climate change, population growth, and resource mismanagement illustrates this urgent global challenge and underscores the need to explore alternative water sources (Mirzavand and Bagheri 2020, Hamidifar 2024, Ghiasi, Aslani et al. 2025).

Atmospheric water harvesting (AWH) represents a promising solution, capitalizing on the approximately 13 trillion tons of water vapor present in the Earth's atmosphere—a volume greater than all the world's river water combined. Notably, the atmosphere retains significant moisture even in arid regions (Kim, Yang et al. 2017, Wang, Liu et al. 2024). Existing AWH strategies can be broadly categorized into passive and active methods. Passive techniques, such as dew and fog harvesting, rely on natural condensation processes but perform optimally only under conditions of high relative humidity. In contrast, active systems employ mechanical or chemical means to condense water vapor, enabling more reliable performance across wider humidity ranges, albeit often at a higher energy cost (Feng, Akther et al. 2022, Zeng, You et al. 2024).

Nomenclature

W_{ad}	Sample weight, g
M_t	Moisture content based on dry weight, g
S_{BET}	BET surface area, m^2/g
S_{lang}	Langmuir surface area, m^2/g
m_{ads}	Mass of adsorbed water per gram of MOF (g/g)
C_p	Specific heat capacity of water (J/g°C)
ΔT	Temperature difference

V	volume of desorbed water per gram of MOF in liters
Qst	Isosteric heat of adsorption (kJ/mol)
R	universal gas constant (J/mol.K)
P	equilibrium vapor pressure (Pa)
T	absolute temperature (K)

Several conventional sorbents, including silica gel, zeolites, and hygroscopic salts, have been employed for active AWH. Silica gel is favored for its low cost and large surface area (100–1000 $m^2 g^{-1}$), yet its strong silica–water interactions necessitate high desorption temperatures (Heidari, Roshandel et al. 2019, LaPotin, Kim et al. 2019). Zeolites, which possess aluminum sites that serve as water adsorption centers, also suffer from high regeneration demands and limited capacity (Wei, Wang et al. 2013, Tatlier, Munz et al. 2018, Sultan, Bilal et al. 2021). Hygroscopic salts (e.g., LiCl, $CaCl_2$, $MgCl_2$) capture atmospheric moisture through hydration processes involving both chemical and physical adsorption. However, their aggregation tendency, poor durability, limited water uptake, and high regeneration energy requirements constrain practical deployment (Asim, Badiei et al. 2021).

Metal–organic frameworks (MOFs) have recently emerged as compelling alternatives for AWH. These porous, crystalline materials consist of secondary building units (SBUs) connected by organic linkers to form two- or three-dimensional framework (Roy, Laha et al. 2019). Their tunable pore size, exceptionally high surface area, and modifiable chemical functionality have enabled applications in separation, purification, catalysis, drug delivery, and gas storage. Through appropriate functionalization, MOFs can be tailored to selectively capture water molecules even at low relative humidity (10–20%), where conventional sorbents typically fail. Furthermore, the crystal structure, particle size, and morphology of MOFs can be precisely controlled through the use of modulators that inhibit uncontrolled crystallization and refine particle characteristics (Zhang, Nai et al. 2017, Meng, Dang et al. 2022). The crystal structure, particle size, and morphology of MOFs can be precisely controlled by modulators to prevent crystallization and modify particle size (Rieth, Yang et al. 2017, Łuczak, Kroczewska et al. 2023).

Several studies have demonstrated the capability of MOFs for atmospheric water harvesting. Ji et al. synthesized an MCM-41/calcium chloride composite, achieving 1.75 kg water/kg adsorbent at 78-92% RH (Ji, Wang et al. 2007). Kumar et al. developed a solar-powered system using silica gel that produced 0.2 liters of water/kg daily (Kumar and Yadav 2015). In a breakthrough study, Yaghi et al. introduced a MOF-801-based device capable of harvesting 2.8 liters of water/kg of MOF at RH < 20%, demonstrating the potential of MOFs for water harvesting in arid environments (Kim, Yang et al. 2017). Yilmaz et al. reported a polymer-MOF blend with MIL-101(Cr), collecting 6.04 g water/g after 1440 hours at 90% RH, exhibiting high delivery efficiency (Yilmaz, Meng et al. 2020). More recently, Yang et al. crystallized MOF-801 on P(NIPAM-GMA) spheres, capturing 1.60 kg H_2O/kg composite/day from 20% RH between 25°C and 85°C (Yang, Wu et al. 2023). Regeneration has also been a challenge, as traditional sorbents like zeolites and hygroscopic salts typically require temperatures above 150 °C, resulting in high energy consumption (Ahrestani, Sadeghzadeh et al. 2023).

MOF-801 shares a similar structure to UIO-66, a zirconium-based microporous crystalline compound consisting of basic units of $Zr_6O_4(OH)_4(–O_2C–CH=CH–CO_2–)_6$ (Rouhani and Ghiasvand 2024). Six zirconium ions are interconnected by eight μ_3 oxygen atoms (four hydroxyl groups and four O^{2-} ions), generating a square coordination. Each SBU is linked to 12 fumarates, and each fumarate is linked to two SBUs, creating a stable 3D network architecture composed of tetrahedral and octahedral cages (Saidi, Ho et al. 2021). Al-fumarate (Basolite A520), analogous to MIL-53(Al), utilizes fumarate linkers to connect aluminum ions, forming one-dimensional chains that are organized into a three-dimensional framework. A $[Al(OH)(O_2C–CH=CH–CO_2)]$-based framework exhibits rhombohedral pore channels (Jeremias, Fröhlich et al. 2014).

This comparative approach provides a foundation for rational material selection in AWH systems optimized for region-specific climate conditions. This study investigated MOF 801 (Zr fumarate) and Al fumarate (Basolite A520) under identical laboratory and field conditions to identify material-specific advantages in atmospheric water harvesting. By correlating pore structure with humidity-dependent behavior and validating long-term cycling stability under real climates (humid Rasht and arid Isfahan), we address a crucial gap in climate-tailored sorbent benchmarking. Both MOFs demonstrate low regeneration temperatures (<100 °C) and strong

hydrolytic stability, with MOF 801 favoring lower RH environments and Al fumarate performing better at higher RH and warmer temperatures.

2. Materials and Methods

2.1. Materials

Aluminum chloride hexahydrate ($AlCl_3.6H_2O$) and zirconium oxychloride octahydrate ($ZrOCl_2 \cdot 8H_2O$) were purchased from Sigma-Aldrich. Fumaric acid ($C_4H_4O_4$), formic acid (HCOOH), acetone, methanol, and N, N-dimethylformamide (DMF) were purchased from Merck.

2.2. Solvothermal synthesis of MOF-801

MOF-801 was synthesized according to the procedure described in previous literature studies with some modifications (Kim 2018). In brief, 1.6 g of $ZrOCl_2.8H_2O$ and 0.58 g of fumaric acid were dissolved in a solvent mixture of DMF and formic acid (20 mL/7 mL) with magnetic stirring for 1 hour. The mixture was then heated at 130 °C for 6 hours. The white precipitate was filtered, washed three times with fresh DMF, and then with methanol, and finally dried in air. The solid was then dried at 150 °C under a vacuum for 24 h to obtain the activated sample.

2.3. Microwave synthesis of Al-fumarate

Al-fumarate synthesized via a microwave-assisted method with DMF, eliminating the need for a modulator. Conventional solvothermal synthesis of Al-fumarate in the presence of a modulator requires 96 hours. In contrast, our microwave synthesis approach provides rapid, uniform heating, significantly shortens reaction times, reduces the need for chemical additives, and enhances sustainability and the potential for large-scale production.

Initially, 2.45 g of $AlCl_3.6H_2O$ was combined with 0.7 g of fumaric acid, followed by 25 ml of DMF. The intended solution was placed in a sealed container and microwaved at 300 watts for 4 minutes, until a white precipitate formed. The sample was centrifuged at 3000 rpm, washed with methanol and acetone, and then dehydrated at 80°C for 1 hour. This was followed by vacuum drying at 150°C for 3 hours. Ultimately, it was dehydrated for one hour at 80°C and then subjected to a vacuum oven at 150°C for 3 hours to yield a white Al-fumarate powder.

2.4. Characterization

Powder X-ray diffraction (PXRD) was measured on a Philips PW1730 X-ray diffractometer (CuKα, λ = 1.5417 Å), scanning over 2θ angles from 2° to 70°, to verify that the correct material and crystal structure of the crystalline phases were obtained. Fourier-transformed Infrared (FTIR) spectra were recorded using a PerkinElmer Spectrum to obtain information about the chemical bonds in the samples. The measurement was performed between 475 and 4000 cm^{-1}. N_2 sorption at 77 K on the Belsorp Mini2 determined the specific surface area (BET) and hydrogen capacity of the samples. Before analysis, the MOF samples were degassed at 120 °C for 2 hours under a dynamic vacuum. The Thermogravimetric analysis (TGA) technique was used to evaluate the thermal stability profile of the samples. TGA of the samples was performed using a TA Q600 system under air flux. A Scanning Electron Microscopy (SEM) (FEI Quanta 2000) was used to observe the particle size, shape, and dispersity. This method captures images using electrons, which offer much higher magnification than optical microscopes. In addition, EDX-MAP analysis was conducted using the FEI model NANOSEM 450.

2.5. Moisture adsorption-desorption studies

This section employs various methods to investigate the moisture adsorption and desorption experiments conducted using MOF-801 and Al-fumarate. At the Iran Research Institute of Petroleum Industry, a supplemental adsorption test was conducted according to ASTM E104 in a constant humidity and temperature environment with 2 g of MOFs. To achieve an exact relative humidity in closed containers, saturated salt/water solutions were used. A saturated salt solution is a thick liquid composed of chemically pure salt dissolved in distilled water. A desiccator containing different concentrations of saturated salt/water solutions was arranged to maintain conditions with constant humidity and temperature. A digital humidity and temperature meter was also placed in the desiccator to measure moisture and temperature. After water vapor was extracted from the sample, the dried items were weighed and placed in a Petri dish within the desiccator, where they adsorbed water vapor from the controlled-humidity environment. The increase in the adsorbent weight served as a criterion for assessing its adsorption capacity. The equation (1) for the water uptake of samples is as follows:

$$W_{ad} = \left(\frac{2M_t}{100}\right) + 2 \quad (1)$$

W_{ad} is the sample weight and M_t is moisture content based on dry weight after the adsorption test. All adsorption tests were conducted over 2 hours.

Over four months and through several adsorption-desorption cycles, 1 g of MOF-801 and Al-fumarate were examined in two distinct laboratories in Rasht and Isfahan. The temperature ranged from 15 to 35°C, and the relative humidity varied from 40% to 100% during the cycles. The MOF was placed on a watch glass. Before starting the first cycle, the MOF layer was heated and dehydrated in an oven at 100°C for one hour. During the day, when the relative humidity was high, the watch glass containing the MOF was left open to the atmosphere, allowing humid air to penetrate the sorption bed and initiate the sorption process. The weight increase method was used to determine the adsorbent's adsorption capacity. The adsorbent was saturated at the end of the 2-hour adsorption period, indicating the maximum adsorption capacity.

A subsequent test was carried out using 2 g of MOF-801 and Al-fumarate. After a 2-hour adsorption period, the samples were sealed in a Pyrex cup without a condenser for the desorption process. Two methods were used for desorption. The initial method used convection in the oven, while the subsequent approach used radiation from a linear halogen lamp to simulate sunlight. The mean desorption temperature was approximately 80 °C, achieved within 2 hours in both methods.

During desorption, the Pyrex cup was sealed, and the temperature of the sorbent bed was then elevated. The released water vapor ultimately condensed into droplets on the interior surface of the Pyrex cup and accumulated at the bottom. The condensed water was collected and weighed, yielding ~0.5 g from 2 g of MOF per cycle, which agrees with the predicted uptake. Although the small sample size (~2 g) limited accuracy, this provides a semi-quantitative validation of the desorption process. During desorption, the MOF layer's temperature increases upon exposure to incoming heat, then returns to its original weight. The images captured during this step are shown in Figure 13.

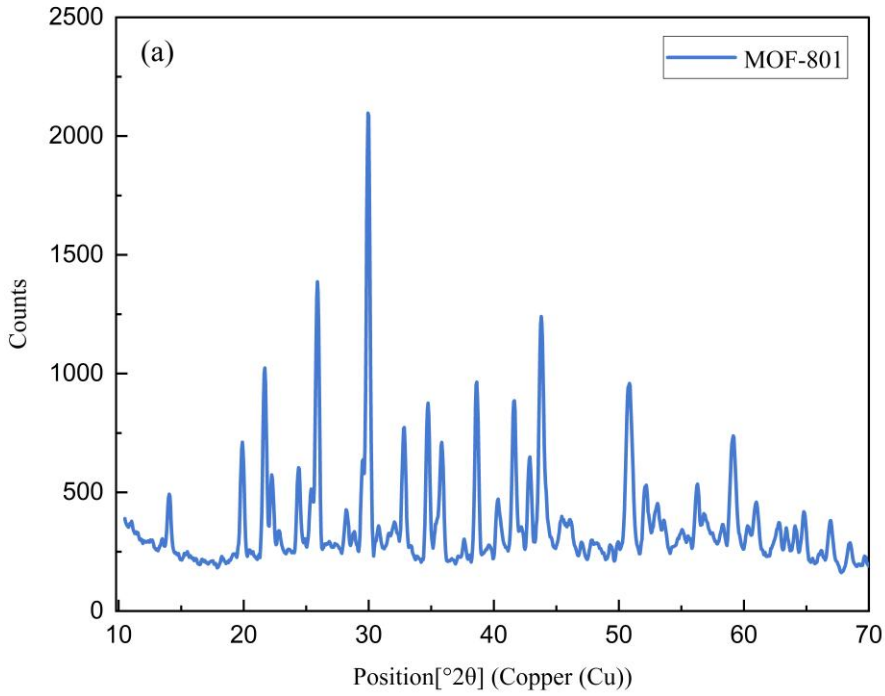
3. Results and discussion

3.1. Structural and textural properties

The vital requirements for effective atmospheric water harvesting (AWH) materials are exceptional adsorption and desorption performance, an appropriate operating pressure range, and robust stability (Ejeian and Wang 2021). In this study, MOF-801 and Al-fumarate were successfully synthesized using fumaric acid as a linker and DMF as a solvent. We demonstrate that these MOFs, with a suitable pore size, are an optimal choice.

Powder X-ray diffraction of MOF-801 and Al-fumarate is shown in Figure 1, which confirms its crystallinity. The XRD patterns of MOF-801 in Figure 1(a) show good reflections at ~10°, 13.9°, 19.9°, and 21.7°, which can be allocated to the (200), (222), (420), and (440) planes. These sharp peaks, indicating a pure, well-structured crystal, correspond to patterns reported in the literature for MOF-801. Al-fumarate nanoparticles in Figure 1(b) have sharp peaks at 10.0°, 15.6°, 18.3°, 21.1°,31.8°, and 43.9°, which are in good agreement with the XRD test results for the reference sample, as an Al-fumarate. The absence of additional peaks indicates that the materials are stable and well-structured. These results confirm the successful synthesis of highly crystalline MOF-801 and Al-fumarate, which are essential for their water adsorption capacity. Therefore, the material's structure is stable because no additional peaks are detected. The FTIR spectra of MOF-801 are presented in Figure 2(a). The first two peaks at 651 cm^{-1} and 794 cm^{-1} can be attributed to asymmetric Zr-O stretching and the vibration of the $Zr_6(OH)_4O_4$ cluster, respectively. The adsorption peak at 1209 cm^{-1} and 985 cm^{-1} indicates -C=O-OH and C-O, respectively. The adsorption at 1399 cm^{-1} is attributed to the symmetric stretching of -C=O-O in a linking carboxyl group, while the asymmetric stretching of this group causes bands at 1579 cm^{-1} and 1657 cm^{-1}, which can be related to the carboxylic acid group of fumaric acid. In addition, a strong adsorption peak at 3221 cm^{-1} was assigned to the stretching vibration of the -OH bond. The FTIR spectrum of Al-fumarate is shown in Figure 2(b). The peak at 3200-3600 cm^{-1} was due to the stretching vibration of water molecules trapped within the Al-fumarate structure. The 1602 cm^{-1} and 1417 cm^{-1} peaks were ascribed to the asymmetric and symmetric stretching of carboxylic groups in fumarate. The peaks at 490-692 cm^{-1} and 805-1093 cm^{-1} were related to the bending and stretching vibration of Al–O. The nitrogen adsorption isotherm at 77 K of the MOF-801 powder sample obtained from the synthesis was distinguished as a type I isotherm (Figure 3(a)), consistent with cage-dominated uptake and early site filling, supporting fast initial adsorption at moderate RH.

Table 1 shows the physical properties of the sample obtained in this work. The Langmuir surface area of the sample determined from the sorption isotherm is 854 m^2g^{-1}, and the BET surface area and total pore volume are 747 m^2g^{-1} and 0.62 cm^3g^{-1}, respectively. The nitrogen adsorption isotherm at 77 K of the Al-fumarate powder sample displays a type II isotherm with an H3 hysteresis loop, indicative of slit-like mesopores formed by plate-like aggregates (Figure 3(b)). The capillary density in these samples is approximately 0.8 P/P0, confirming that they have a high porosity. The hysteresis is relatively narrow and is dedicated to reversible and continuous pore-filling. H3 loops arise from slit-shaped pores and network effects, in which condensation/evaporation hysteresis and percolation lead to delayed pore emptying relative to adsorption, aligning with accelerated uptake at high RH in Al-fumarate. The BET surface area and total pore volume are 48 m^2g^{-1} and 0.066 cm^3g^{-1}, respectively. Pore size distribution analysis (Figure 3(c) and 5(d)) shows a peak pore diameter of 1.29 nm for MOF-801 (microporous) and 4.65 nm for Al-fumarate (mesoporous). The significantly higher surface area of MOF-801 suggests a greater number of adsorption sites, while the mesoporous structure of Al-fumarate may facilitate faster water diffusion. For the Zr-fumarate sample, the N_2 adsorption isotherm corresponds to a type I behavior, which is characteristic of a microporous material. The adsorption plateau indicates that uptake is governed mainly by the volume of accessible micropores rather than by the total external surface area. The BET surface area of Zr-fumarate is 747.89 $m^2\ g^{-1}$, with an average pore diameter of 3.31 nm and a total pore volume of 0.622 $cm^3\ g^{-1}$. The adsorption kinetics of these MOFs are strongly humidity dependent, and that multilayer formation becomes more important at higher relative humidity because of water–water interactions in addition to water–framework interactions. The higher adsorption-rate constants observed for Al-fumarate relative to Zr-fumarate are consistent with its stronger tendency toward multilayer adsorption under humid conditions. This behavior is intrinsic to the Al-fumarate framework chemistry and helps explain why the sample can still show meaningful water uptake despite its low measured BET area.



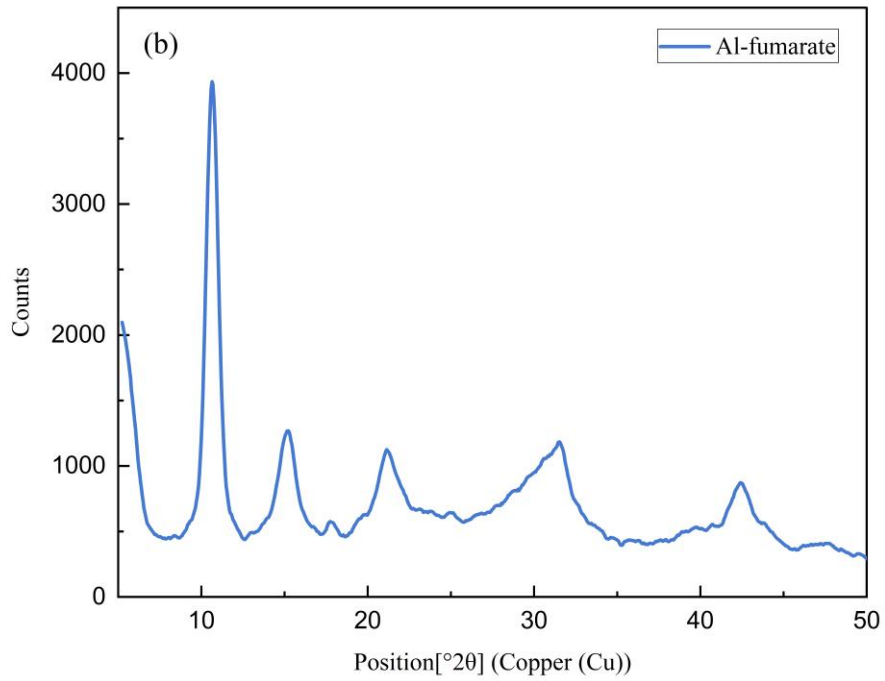
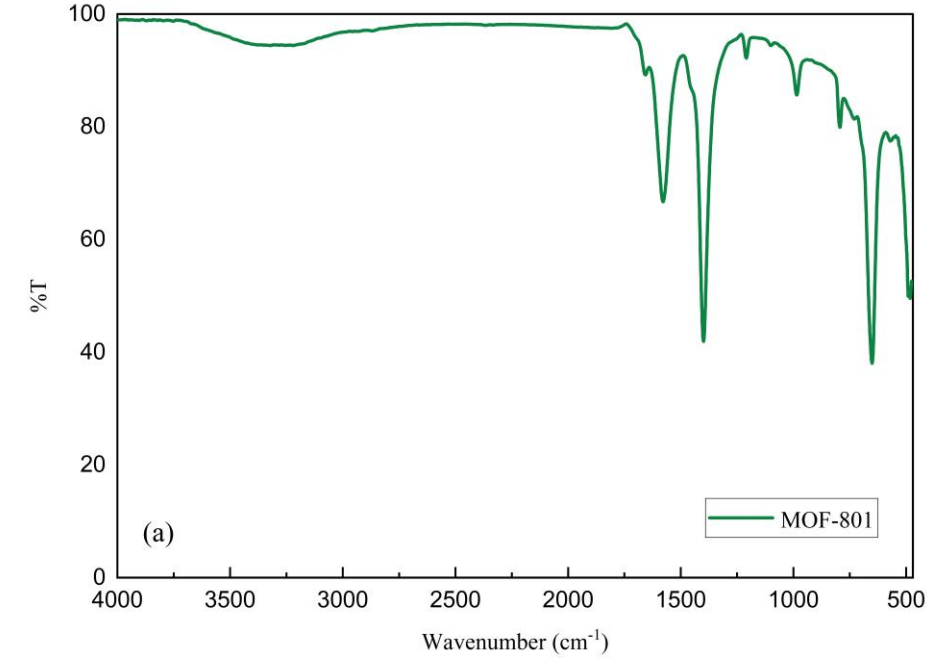


Figure 1. XRD patterns of synthesized samples, (a) MOF-801 and (b) Al-fumarate



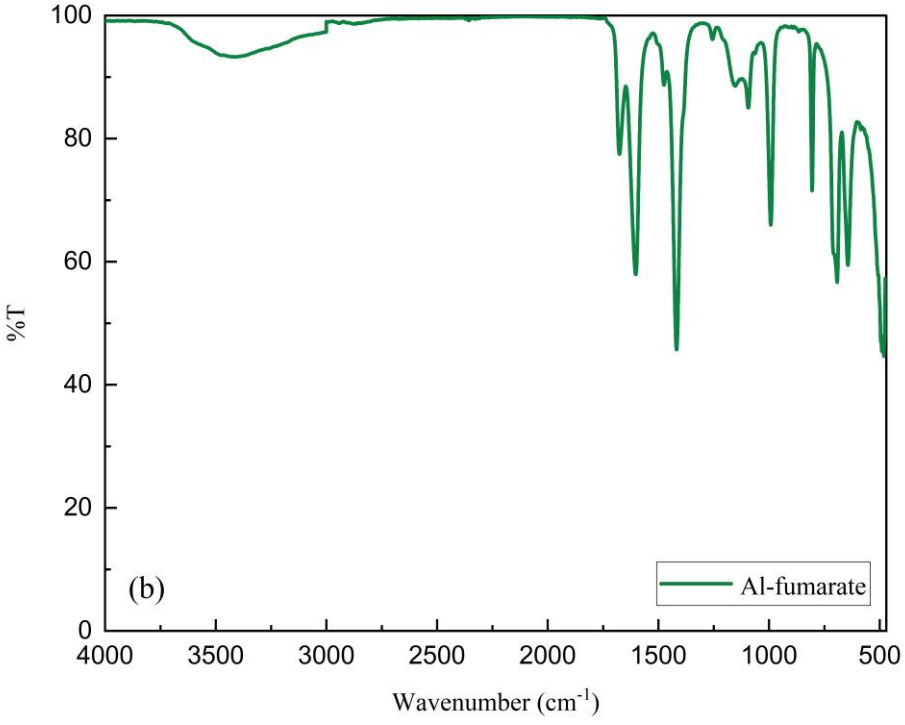
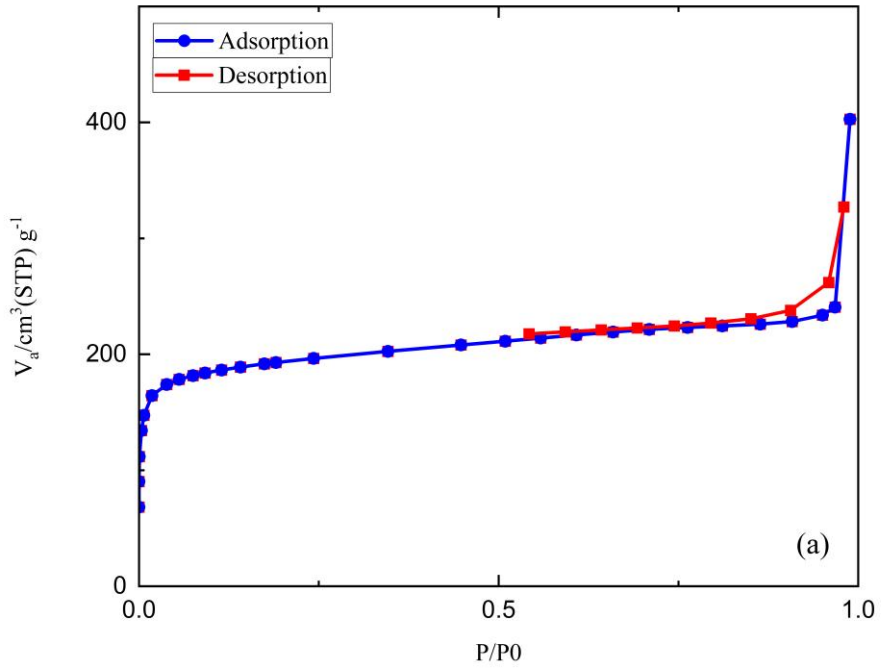
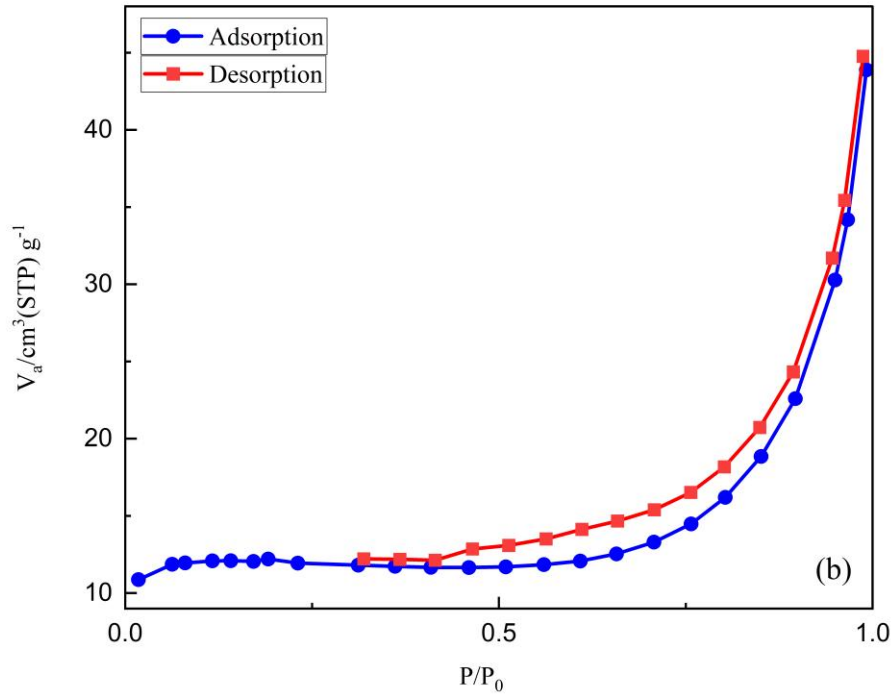


Figure 2. FTIR spectrum of (a) MOF-801 and (b) Al-fumarate


Adsorption
Desorption
400
200
0
0.0
0.5
1.0
P/P0
V_a/cm^3(STP) g^{-1}
(a)


Adsorption
Desorption
40
30
20
10
0.0
0.5
1.0
P/P$_0$
V_a/cm^3(STP) g^{-1}
(b)

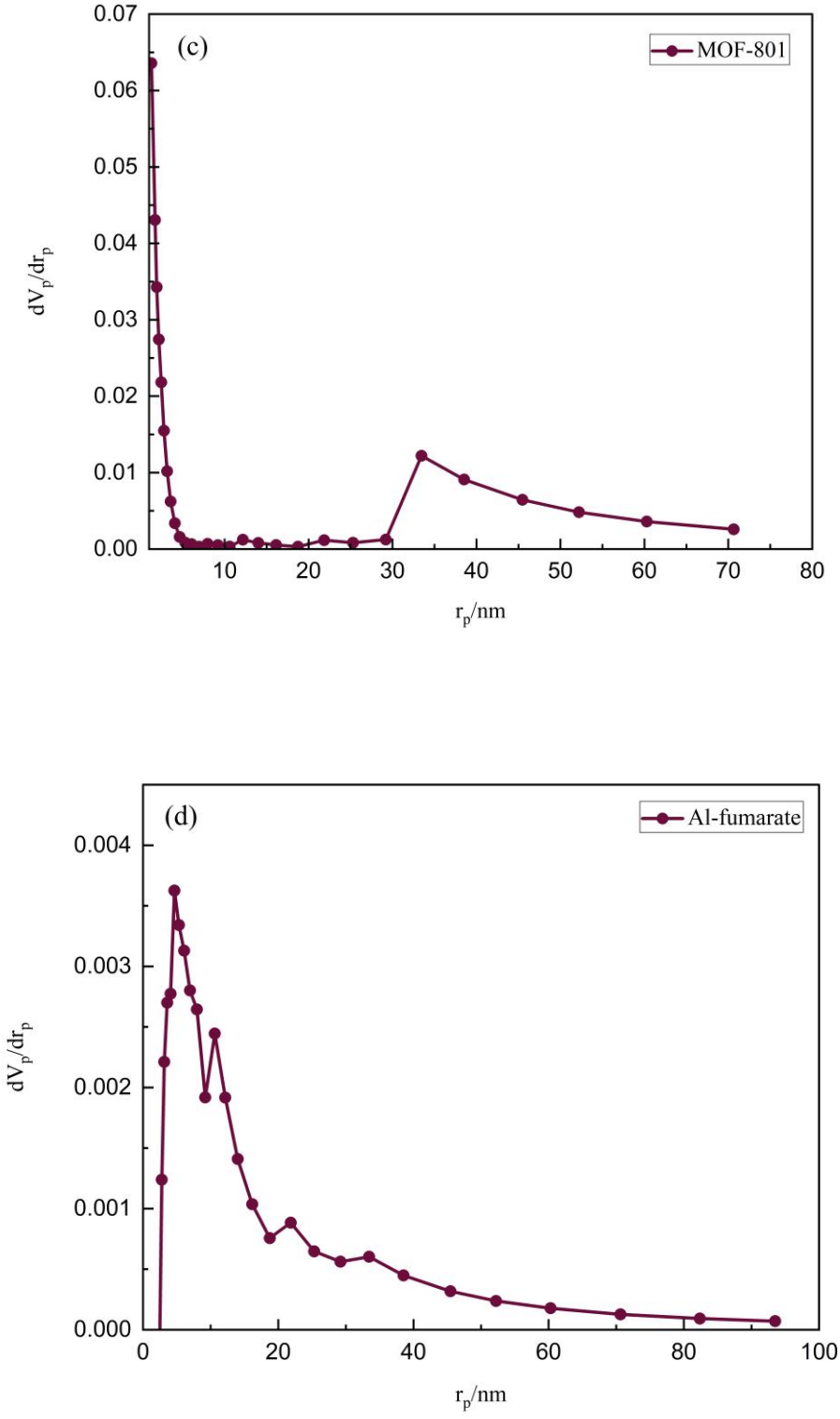


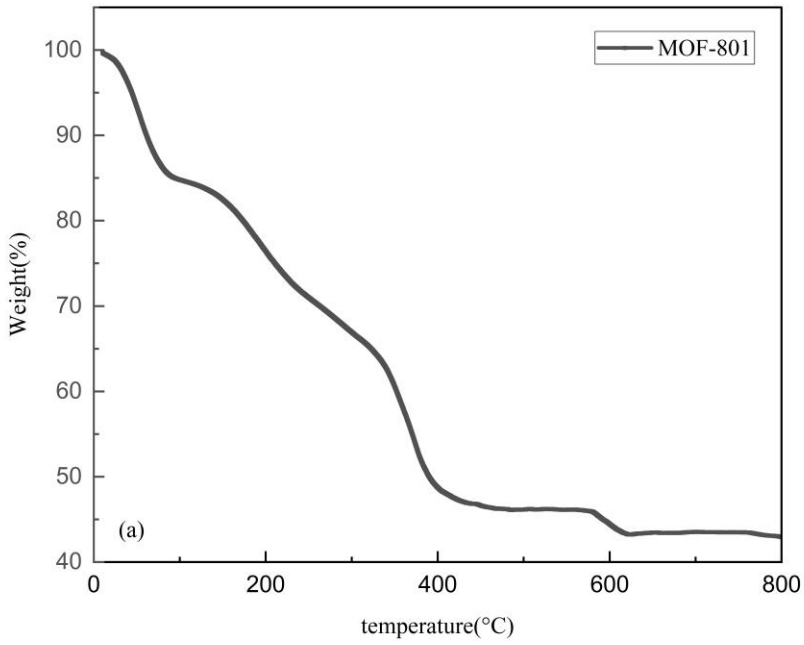
Figure 3. N_2 sorption isotherm at 77 K, (a) MOF-801 and (b) Al-fumarate. (c) pore size distribution of MOF-801, (d) pore size distribution of Al-fumarate

Table 1. Physical properties of MOF-801 and Al-fumarate sample

	$S_{BET}(\mathbf{m^2g^{-1}})$	$S_{lang}(\mathbf{m^2g^{-1}})$	Pore volume($\mathbf{cm^3g^{-1}}$)
MOF-801	747	854	0.62
Al-fumarate	48	52	0.066

Figure 4(a) displays the TGA curve of MOF-801 under airflow. TGA analysis can determine the optimum temperature at which samples can be degassed without decomposition. The weight-loss profile from the thermogravimetric analysis of Zr-MOF exhibits three main stages of weight loss over 0-800°C. The first stage corresponds to a temperature of 80°C, at which the endothermic thermal desorption of water molecules from the pores occurs. The second one, which happens at 400°C, corresponds to an exothermic reaction. This weight loss likely refers to breaking the coordinated bonds between the SBUs and fumarate linkers, as well as removing all organic material, including the evaporation of guest molecules from the pores, such as DMF. Between 400 and 600°C, the weight loss was almost linear, suggesting the high thermal stability of the synthesized sample. The last one, at 600 °C, also belongs to the exothermic process, attributed to the decomposition of the carbon shells and the formation of the final product, pure ZrO_2. The TGA profile of MOF-801 is quite similar to the previously reported data. Both retained their structure up to 600 °C, indicating the highly crystalline nature of the Zr-MOF, with high thermal stability. Physical and chemical changes in the Al-fumarate structure with temperature changes can be observed in the TGA curve in Figure 4(b). It is clear from this curve that in the temperature range of 35 to 100°C, the adsorbed H_2O molecules were removed. The product lost 65% of its weight in the first step in the 380-550 °C temperature range. It was due to the thermal degradation of fumaric acid, coordinated with aluminum oxide clusters. The remaining 35% of the sample weight above 550°C was probably aluminum oxide. This graph shows that Al-fumarate has thermal stability up to 380 °C, consistent with previously reported data. SEM images of the sample show particles with a size of approximately 200 nm, as shown in Figure 5. The synthesized MOF-801 particles, with crystallized octahedral structures, exhibit good dispersity and monotonous size distribution. These images are also consistent with other observations reported in a previous article. SEM images in Figure 6 show Al-fumarate particles with a diameter of approximately 200 nm and a tetrahedral shape. The images are synchronized with the molecular structure of Al-fumarate. Hence, this

ascertains that it is correctly synthesized. It is also observed that the particles have strong aggregation, which is very similar to the structure of MOF-801.



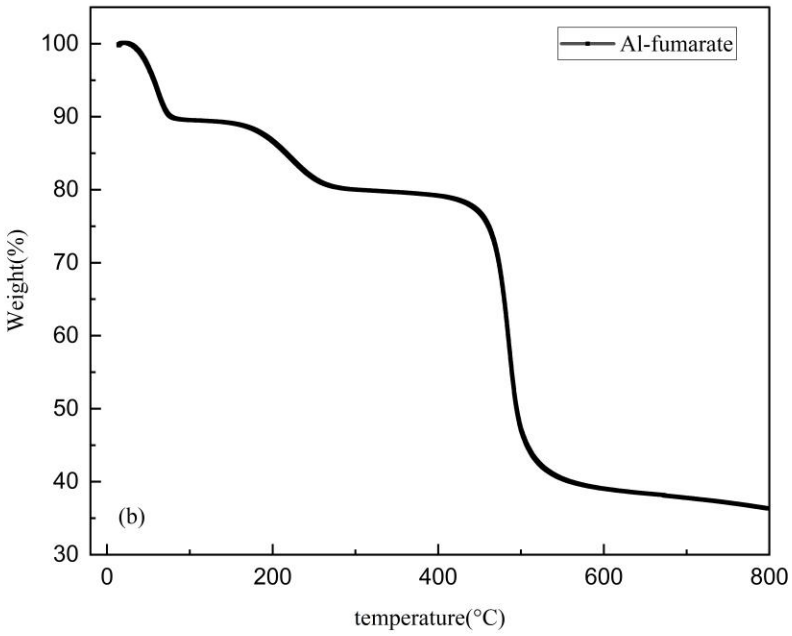


Figure 4. TGA curve, (a) MOF-801 and (b) Al-fumarate

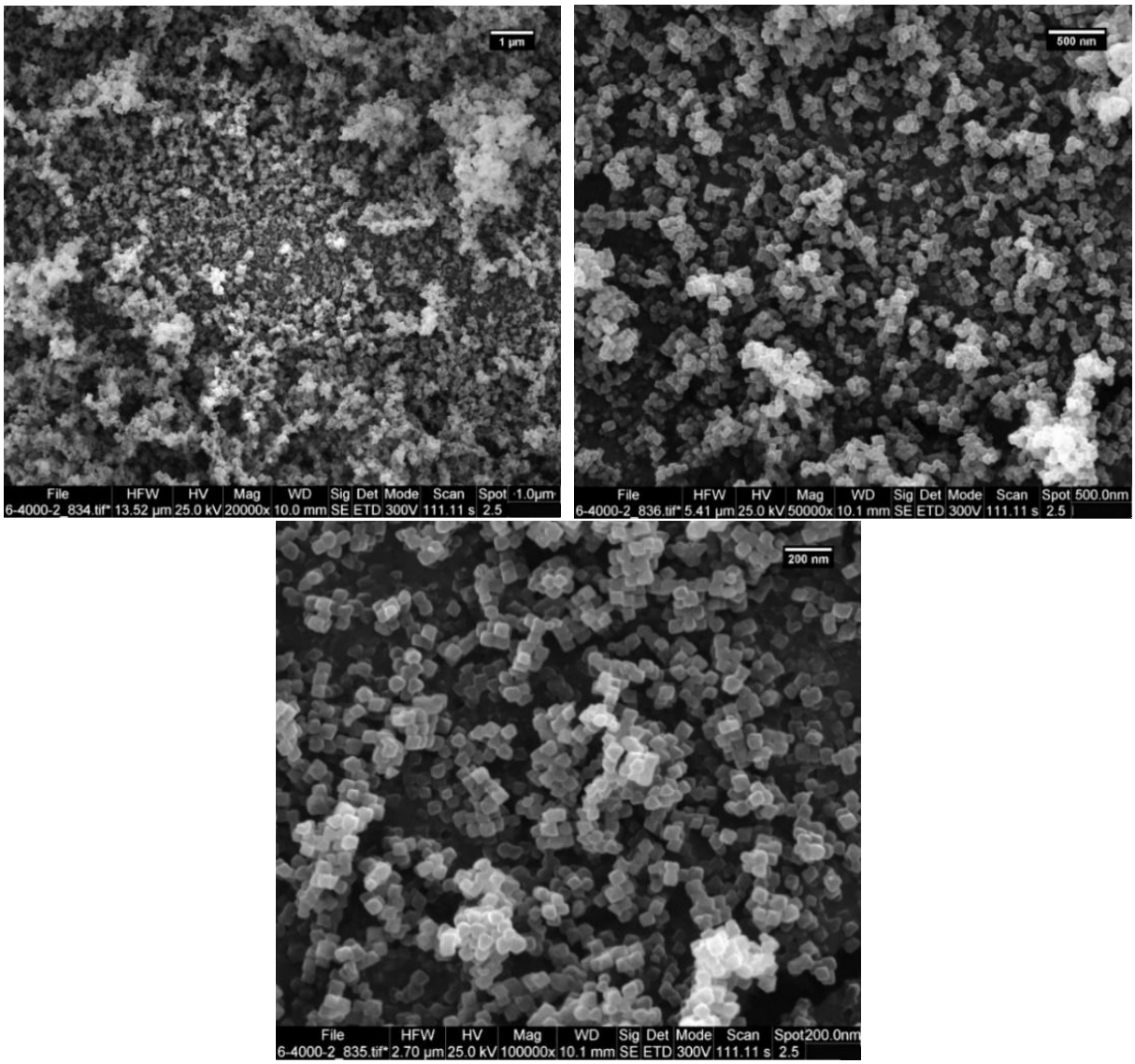


Figure 5. SEM images of MOF-801

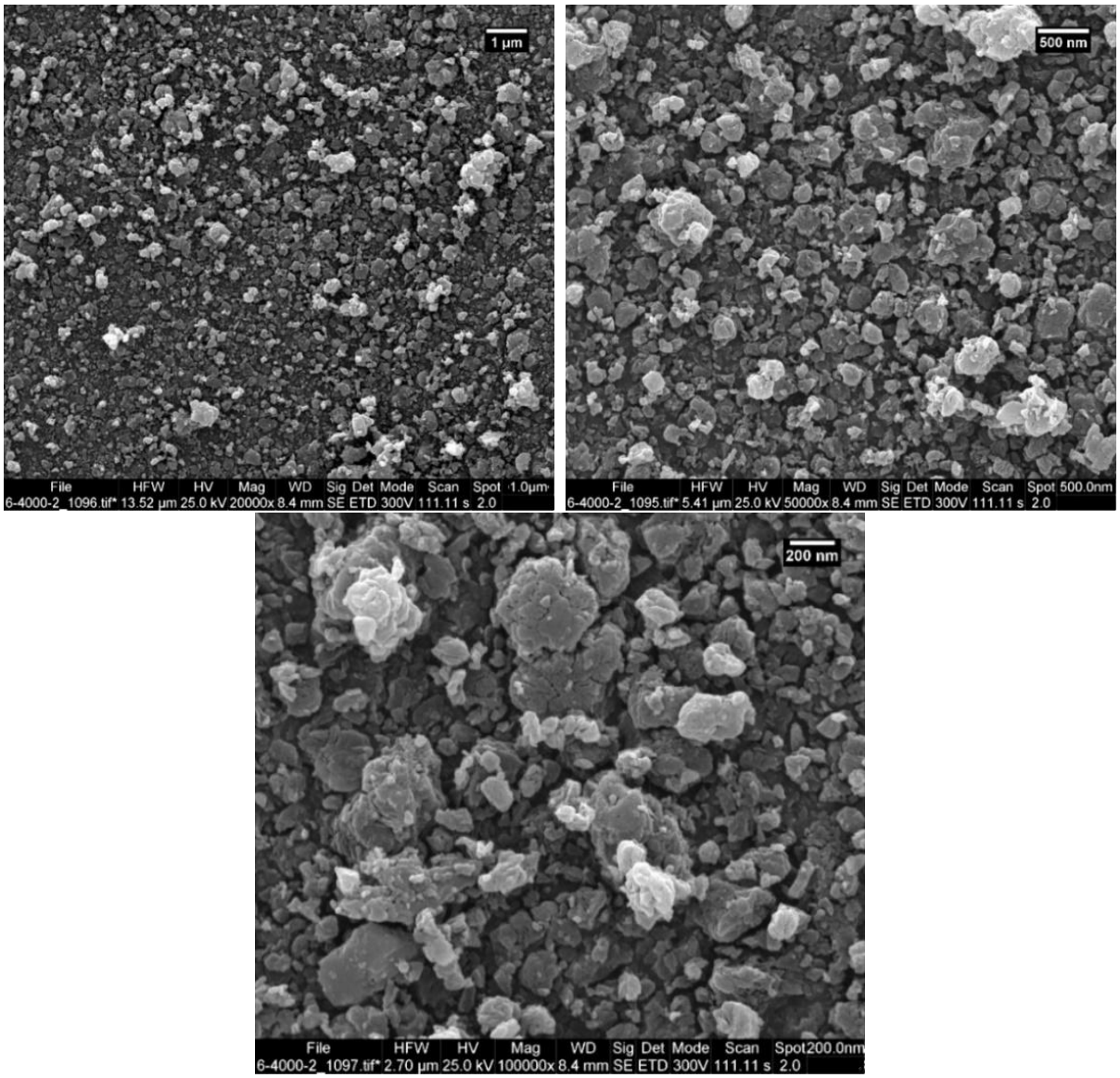


Figure 6. SEM images of Al-fumarate

EDX mapping was done to analyze the elemental composition of the MOF-801. The blue, red, green, and yellow dots represent carbon, oxygen, zirconium, and nitrogen, respectively, compatible with the elements in the crystal. According to Figure 7, the zirconium element has the highest dispersion in the MOF-801 structure. To better confirm the presence of Al-fumarate nanoparticles, elemental mapping analysis was performed, and the results are shown in Figure 8. The colors blue, green, red, and yellow identify the elements carbon, aluminum, oxygen, and

nitrogen. This diagram confirms the presence of aluminum ions as the main element of Al-fumarate nanoparticles.

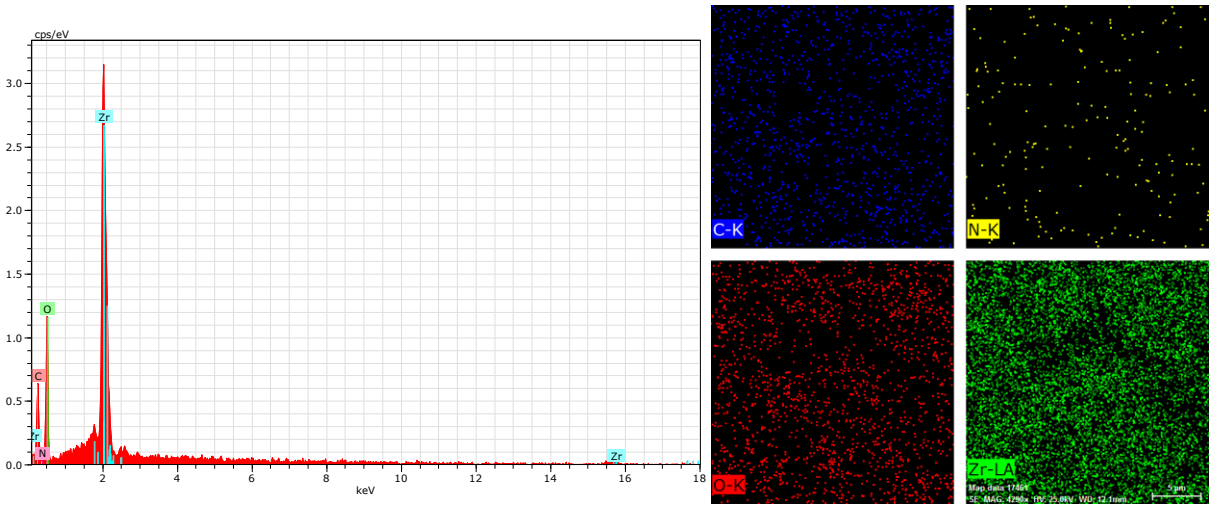


Figure 7. EDX-Mapping analysis of MOF-801

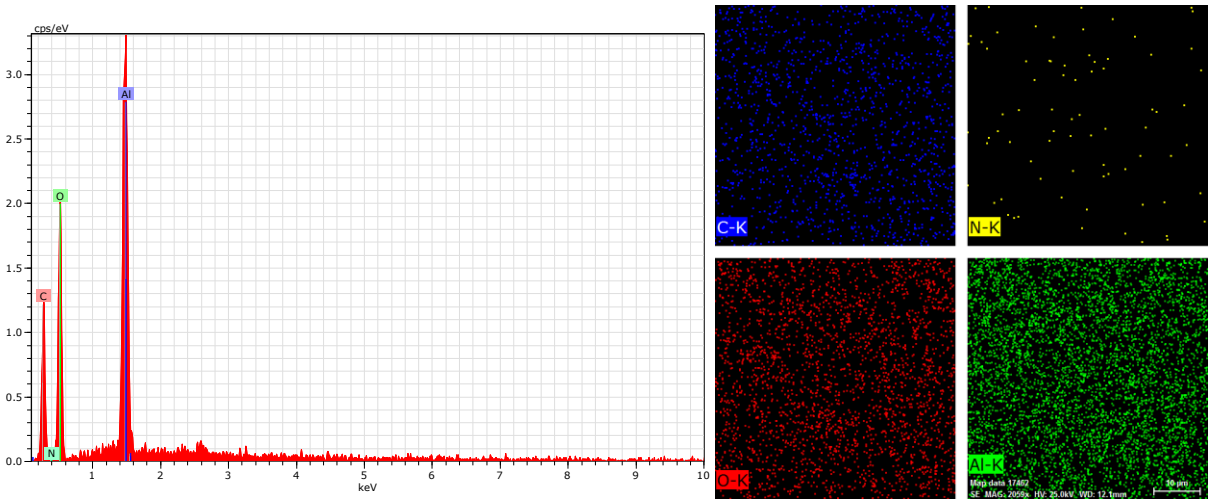


Figure 8. EDX-Mapping analysis of Al-fumarate

3.2. Water uptake behavior (lab ASTM tests)

To further investigate the adsorption behavior of MOF-801 and Al-fumarate, experiments were conducted in accordance with ASTM E104 standards under controlled temperature and humidity conditions. Using 2g of each MOF, the following results were observed. Figures 9 and 10 illustrate the nuanced performance characteristics of MOF-801 and Al-fumarate under varying relative humidity (RH) and temperature conditions, which are crucial for atmospheric water harvesting

(AWH) applications. While MOF-801's efficacy hinges on a balance of favorable humidity and temperature, Al-fumarate exhibits notable responsiveness to RH fluctuations, potentially indicating a more adaptable adsorption mechanism attributed to its mesoporous structure, facilitating enhanced capillary condensation. The results in Table 2 show the water uptake (g H_2O/2 g MOF) of both materials at 20°C and 25°C, with relative humidity (RH) levels of 40%, 60%, and 80%, over adsorption times of 30 minutes, 1 hour, and 2 hours. The observations demonstrate a clear association between increased relative humidity and enhanced water adsorption capacity in MOF-801 and Al-fumarate. As shown in Table 2, for MOF-801, the adsorption capacity at 40% RH is 0.34 after 30 minutes at 20 °C, and it increases to 0.396 at 60% RH. When the RH rises to 80%, the adsorption capacity considerably grows to 0.526. After 2 hours, the adsorption capacity reaches 0.494, 0.548, and 0.608, respectively.

Similarly, for Al-fumarate, at 40% RH, the material adsorbs 0.32 g of water at 20°C after 30 minutes, increasing to 0.432 g after 2 hours. It is observed that, at 80% RH, the adsorption capacity increases markedly to 0.558 after two hours at 20°C. Such a phenomenon can be illustrated by the increased availability of water molecules in the atmosphere at elevated humidity levels; hence, materials can adsorb greater amounts of moisture within their porous structure. MOF-801 and Al-fumarate exemplify this trend; however, MOF-801 generally exhibits a higher uptake under these conditions, reflecting its higher affinity for water adsorption across various relative humidity levels. This feature is significant for water harvesting applications where relative humidity fluctuates throughout the day. MOF-801 would adsorb more water during early morning hours, when humidity is elevated, than during arid daytime hours. The excellent performance at elevated humidity levels is attributed to MOF-801's pore architecture and extensive surface area, which facilitate the adsorption of additional water molecules as they become accessible. This characteristic enables MOF-801 to be highly active during water harvesting from the atmosphere, even at very low relative humidity, which is critical in its application in arid areas (Kim 2018). The superior performance of MOF-801 is likely due to its significantly higher surface area, which provides more sites for water molecules to adsorb. At lower temperatures, the adsorbate molecules have lower kinetic energy and tend to stick to these sites, leading to stronger adsorption. At higher temperatures, the increased kinetic energy of adsorbate molecules weakens their interactions with the surface.

The stability of the MOF structure itself becomes essential. Al-fumarate, despite having a lower surface area, might have stronger binding sites or a more thermally robust structure, allowing it to maintain its adsorption capacity better at elevated temperatures. The mesoporous nature can also facilitate diffusion at higher temperatures, allowing the adsorbate to reach the active sites. As shown in Table 3, these benchmarking data position the temperature- and humidity-dependent uptake of MOF-801 and Al-fumarate within a broader performance–scalability context, clarifying how working capacity at relevant RH–T intersects with synthesis practicality and regeneration requirements. Although MOF-303 exhibits higher water uptake (~0.4 g/g at 20% RH), it relies on costly linkers and a multistep synthesis, which constrain scale-up and limit device-level feasibility in resource-constrained settings. In contrast, Al-fumarate and MOF-801 offer a balanced profile that combines competitive adsorption with hydrolytic/thermal robustness, abundant and non-toxic metal centers, and regeneration at temperatures below 100 °C, thereby aligning material performance with manufacturability and energy efficiency. Taken together, the comparative evidence and the observed uptake kinetics support prioritizing MOF-801 and Al-fumarate as pragmatic sorbents for sustainable, large-scale atmospheric water harvesting across various climatic regimes.

Table 2. The adsorption capacity of MOF-801 and Al-fumarate during 2 hours

		20 °C			**25 °C**		
		30 min	1 hr	2 hr	30 min	1 hr	2 hr
MOF-801	40% RH	0.34	0.478	0.494	0.266	0.27	0.298
	60% RH	0.396	0.508	0.548	0.342	0.388	0.392
	80% RH	0.526	0.588	0.608	0.358	0.414	0.408
Al-Fumarate	40% RH	0.32	0.424	0.432	0.318	0.418	0.484
	60% RH	0.356	0.5	0.522	0.35	0.5	0.518
	80% RH	0.468	0.554	0.558	0.46	0.552	0.556

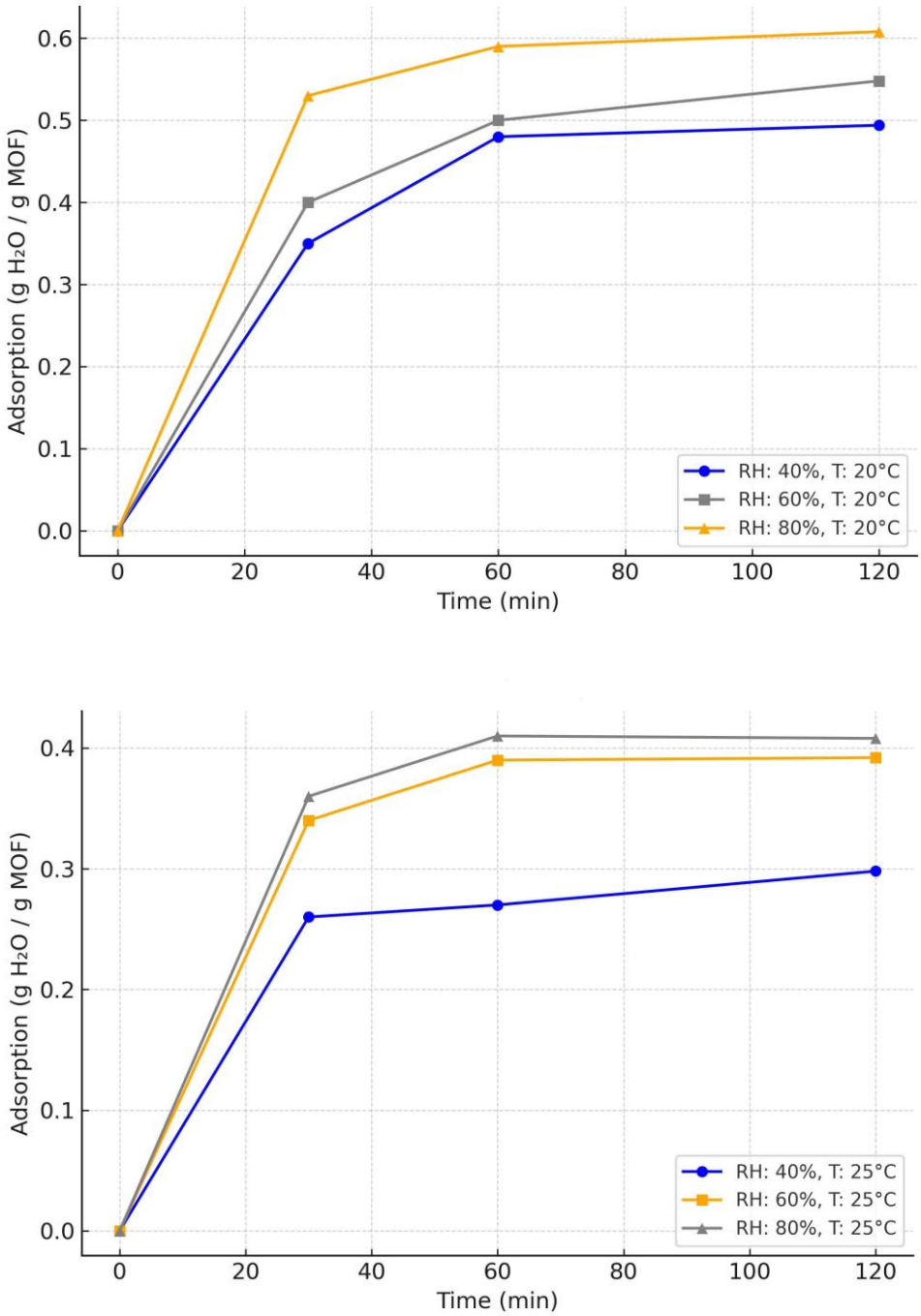


Figure 9. Adsorption rate of MOF-801 in different RH and temperature conditions in 2 hours

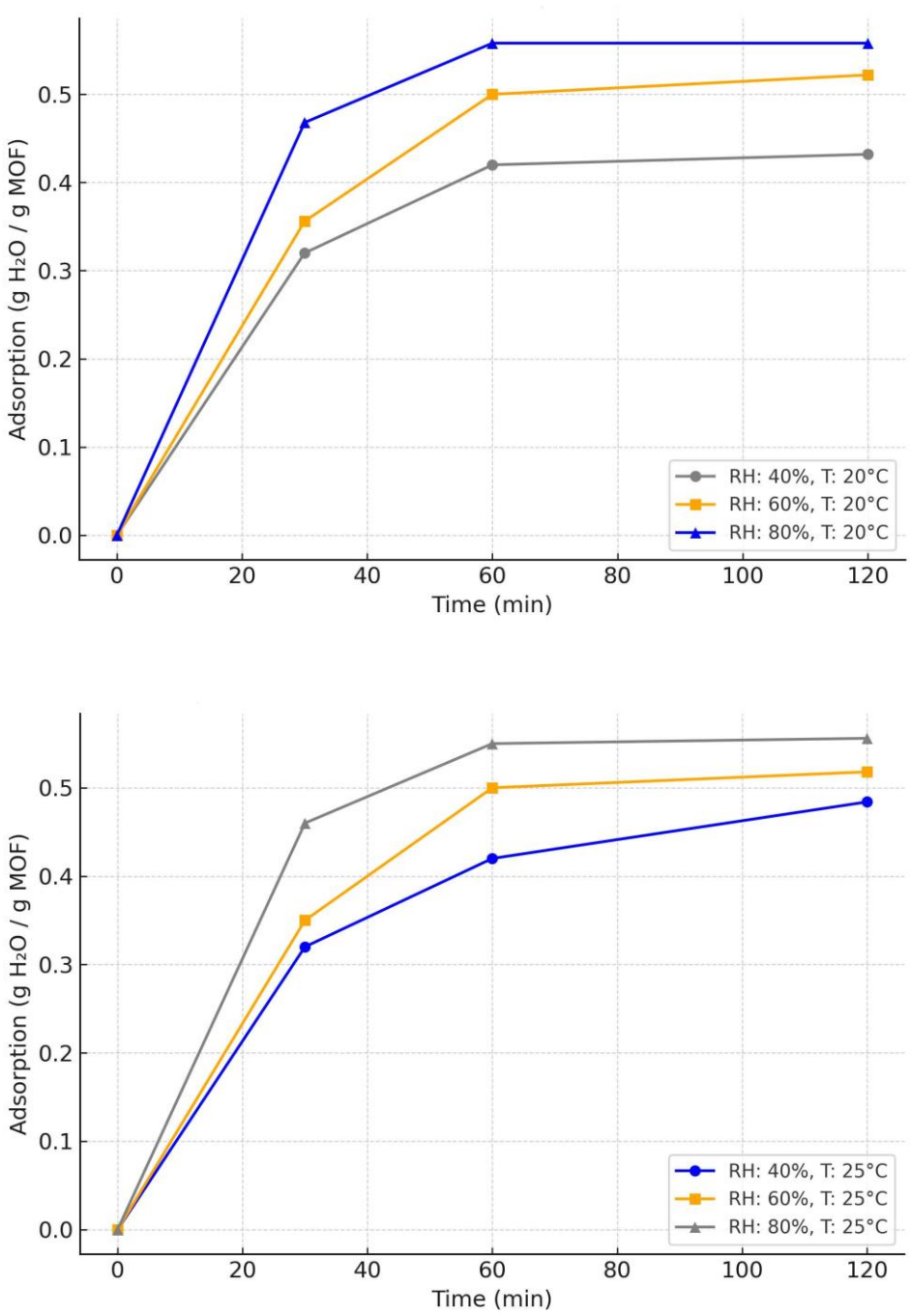


Figure 10. Adsorption rate of Al-fumarate in different RH and temperature conditions in 2 hours

Table 3. Comparative water uptake of sorbents for atmospheric water harvesting

Material	Water uptake (g H_2O/g)	RH (%)	Temperature (°C)	Reference
MOF-801	0.247	40	20	This work
Al-fumarate	0.216	40	20	This work
MOF-303	0.40	20	30	(Kim, Yang et al. 2017)
MIL-101 (Cr)	0.20	~50	25-30	(Logan, Langevin et al. 2020)
Zeolite 13X	0.18	60	30	(Hanikel, Prévot et al. 2019)
Silica gel	0.20	80	25	(Mulchandani, Malinda et al. 2020)

Water molecules move as a gaseous flow in pores with a diameter (D) exceeding the mean free path of water molecules (λ, approximately 85 nm in dry air). In such cases, the frequency of collisions between water molecules is significantly higher than that between water molecules and the pore wall. It leads to the pore architecture having a negligible influence on the diffusivity of water molecules, particularly under conditions when $D \gg \lambda$. When the pore diameter is decreased to a value lower than the mean free path of the molecules, water molecules will be more likely to collide with the pore walls than to move in the available space freely. It gives rise to Knudsen flows, in which these collisions strongly influence the motion of water molecules. When the pore wall strongly attracts water molecules, surface flow transport often occurs more slowly than gaseous transport. At lower P/P_0 water populates high-affinity sites and forms a primary monolayer. As P/P_0 increases secondary hydrogen-bonded layers, and capillary condensation proceeds in mesopores. MOF-801's microporous framework favors rapid primary-site filling (monolayer-dominated at moderate RH). At the same time, Al-fumarate's slit-like mesopores promote multilayer adsorption and capillary condensation at elevated RH, consistent with the

observed H3 hysteresis. This is owing to increased collisions of water molecules with the pore wall and increased interactions with –OH groups within the structure. In this hydrophilic, porous adsorbent, water is initially adsorbed at the primary hydrophilic sites via bonding. Water molecules associate with the zirconium SBUs via interactions with -OH and carboxyl groups, followed by a second phase in which water molecules form hydrogen bonds with primary adsorbed molecules, ultimately leading to the formation of water clusters. Primary molecules constitute additional adsorption sites that permit the growth of interconnected clusters. Similarly, water adsorption initiates in the hydrophilic pores of Al-fumarate, with preferential nucleation at hydrophilic and polar sites, and the clustering of water molecules then begins. The pores in Al-fumarate are larger than those in MOF-801, and the interaction of water with hydrophilic functional groups occurs later, allowing the pores to be filled later. Additionally, because the critical diameter of this adsorbent exceeds that of water, capillary condensation occurs, as evidenced by the hysteresis loop in the BET diagram.

The adsorption performance of MOF-801 and Al-fumarate is also significantly influenced by temperature. The data for MOF-801 indicate that water adsorption decreased slightly as the temperature increased. For example, the adsorption capacity is 0.494 at 20°C and 40% RH, and it decreases to 0.298 after 2 hours at 25°C. Similarly, the capacity decreases from 0.608 at 20°C and 80% RH to 0.408 at 25°C. However, aluminum fumarate shows stable adsorption when the temperature rises. Al-fumarate would be more suitable in warmer climates, as increased molecular diffusion at those temperatures tends to capture more water. With rising temperature, water molecules gain greater velocity, quickly penetrating the pores and colliding more frequently with the pore walls. This suggests that Al-fumarate acts more efficiently in a slightly warmer environment and, therefore, is a suitable candidate for water harvesting in warm climates. These results align with previous studies, which show that MOF adsorption behavior can vary with temperature due to changes in molecular diffusion and interaction strengths (Zhao, Li et al. 2020).

3.3. Cyclic stability (field tests)

Figure 11 displays the cyclic water adsorption behavior of MOF-801 and Al-fumarate over 40 cycles, demonstrating their exceptional performance and stability for water adsorption. Both materials retained over 95% of their initial water uptake after 40 cycles, outperforming traditional zeolites that typically lose capacity (Xu and Yaghi 2020).

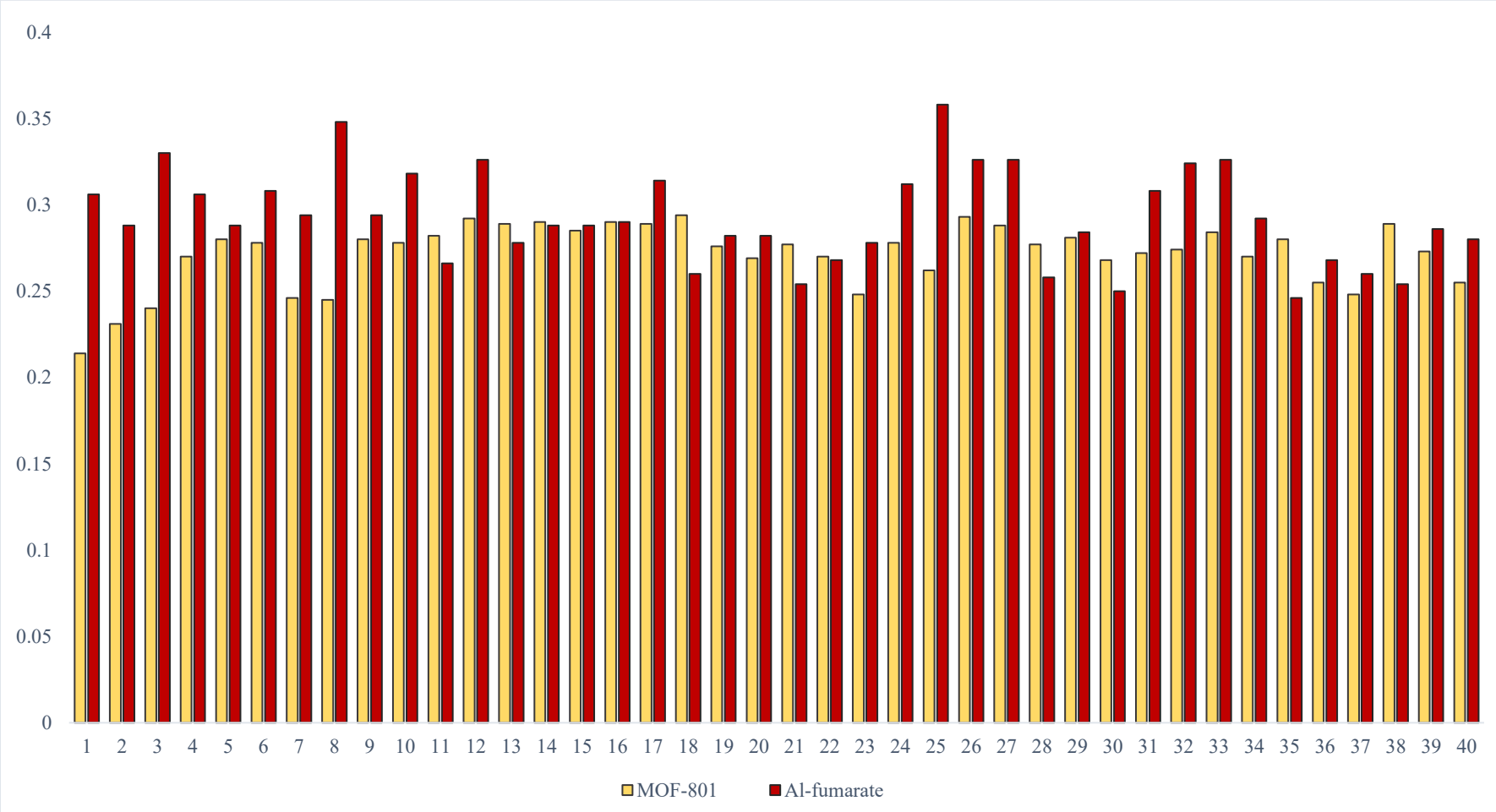


Figure 11. Water sorption behavior of MOF-801 and Al-fumarate in 40 cycles in Rasht and Isfahan at different RH and temperature

MOF-801 consistently exhibits a measurable but relatively lower water adsorption capacity across the 40 cycles, averaging approximately 0.25 g H_2O/g MOF. It suggests that its structural properties may limit the adsorption mechanism in MOF-801. Given the cyclic nature of the experiment, the consistent adsorption suggests a relatively stable interaction between water molecules and the available adsorption sites. A plausible mechanism involves the monolayer adsorption of molecules on specific, high-affinity sites within the MOF-801 structure. Despite the wide RH range, the relatively lower adsorption capacity suggests that either the pore size of MOF-801 limits the number of water molecules it can accommodate or that the number of high-affinity binding sites is limited. The relatively small variation in adsorption capacity across the cycles suggests that the MOF-801 structure is stable under the tested conditions and experiences minimal degradation or irreversible water binding.

In contrast, Al-fumarate consistently demonstrates a higher water adsorption capacity, averaging approximately 0.30 g H_2O/g MOF. It suggests a potentially different adsorption mechanism compared to MOF-801. This observation aligns with the fundamental adsorption mechanism study by Ghasemzadeh et al. (Ghasemzadeh 2025), where a thermodynamic analysis revealed stronger water interactions in Al-Fumarate's mesoporous framework (-43.2 kJ/mol) compared to MOF-801's microporous structure (-28.1 kJ/mol). Their fractal dimension analysis, conducted through the FHH model, further confirmed distinct pore-filling mechanisms between the two materials. The higher uptake could indicate a combination of factors, including a larger pore volume, a greater number of active adsorption sites, or a stronger interaction between water molecules and the Al-fumarate framework. The fact that this higher adsorption is consistent across the range of RH values is essential. The data is not an adsorption isotherm, so we cannot comment directly on the affinity. However, a plausible mechanism could involve a combination of monolayer adsorption on high-affinity sites, as in MOF-801, and multilayer adsorption within the larger pores of the Al-fumarate structure. Given the varying temperature and RH conditions, variations in adsorption capacity are observed across cycles, with Al-fumarate tending to exhibit a higher response (increasing when conditions are favorable and decreasing when less favorable) than MOF-801.

3.4. Thermodynamic and energy analysis

To further elucidate the adsorption behavior of MOF-801 and Al-fumarate, the isosteric heat of adsorption (Q_{st}) was used as an indicator of the strength of water–framework interactions. The Clausius–Clapeyron relation provides a convenient approach to evaluate Q_{st} from adsorption isotherms measured at different temperatures, according to equation (2):

$$Q_{st} = -R\left(\frac{\partial \ln P}{\partial\left(1/T\right)}\right)_q \quad (2)$$

Where R is the universal gas constant, P is the equilibrium vapor pressure at a given loading, T is the absolute temperature, and q represents the amount of water adsorbed. By plotting lnP as a function of $1/T$ at constant uptake, the slope of the resulting line yields the corresponding isosteric heat (Hamid, Vyawahare et al. 2023).

In the context of AWH, Q_{st} is a critical parameter since it directly reflects the energy penalty associated with desorption. Materials with high Qst values typically have stronger binding sites, which can enhance water uptake under arid conditions but may require more energy for regeneration. Conversely, lower Q_{st} values indicate weaker binding, favoring facile desorption but often leading to reduced uptake at low humidity levels.

Applying this framework, one would expect MOF-801, with its smaller pore size and higher affinity for water molecules, to exhibit higher Q_{st} values at low relative humidity, consistent with its superior performance under dry conditions. In contrast, Al-fumarate is anticipated to exhibit lower initial Q_{st} values, consistent with multilayer adsorption and improved performance in humid environments. Although experimental determination of Q_{st} requires adsorption isotherms at multiple temperatures, this thermodynamic perspective reinforces the mechanistic interpretation of climate-specific sorption behavior. It provides a pathway for rational materials selection in future AWH studies.

The thermodynamic perspective provided by the Clausius–Clapeyron relation offers valuable context to the energy efficiency analysis. The higher initial isosteric heat of adsorption observed for MOF-801 reflects the presence of strong binding sites, explaining its superior performance under arid conditions and also implying a greater energy demand for complete

regeneration at low humidity. In contrast, the lower and more uniform Q_{st} profile anticipated for Al-fumarate indicates weaker binding and multilayer adsorption, which facilitates desorption and aligns with its favorable behavior in humid environments. These findings confirm that the two materials exhibit distinct humidity-dependent adsorption regimes rather than contradictory thermodynamic behavior (Ghasemzadeh 2025). These complementary thermodynamic trends demonstrate that regeneration at 80 °C remains feasible for both frameworks while highlighting their climate-dependent suitability. Together, the adsorption energetics and energy balance emphasize the importance of tailoring sorbent selection to regional climatic conditions when designing atmospheric water harvesting systems.

The comparative thermodynamic analysis (Figure 12) highlights the distinct adsorption energetics of MOF-801 and Al-fumarate. At low water loadings, MOF-801 exhibits a markedly higher isosteric heat of adsorption Q_{st}, indicating the presence of strong hydrophilic sites that favor water capture under arid conditions. However, Q_{st} decreases progressively with increasing uptake, reflecting the saturation of primary sites and the subsequent occupation of weaker-binding regions. In contrast, Al-fumarate displays a lower and more uniform Q_{st} profile, consistent with multilayer adsorption and weaker sorbent–adsorbate interactions. This flatter trend suggests that Al-fumarate is more efficient in humid environments, where water uptake can proceed with minimal energetic penalty. These complementary behaviors not only explain the experimentally observed climate-dependent performance but also reinforce the energy analysis, confirming that both frameworks can be regenerated at low temperatures while offering distinct advantages under different atmospheric conditions.

Using adsorption isotherms measured at 20 and 25 °C, we computed the isosteric heat of adsorption Q_{st} by applying the Clausius–Clapeyron relation. The resulting Q_{st} (q) profiles indicate that MOF-801 has higher initial Q_{st} (~50–60 kJ·mol^{-1} at low loadings), consistent with strong hydrophilic binding sites, while Al-fumarate shows lower and more uniform Q_{st} (≈40–45 kJ·mol^{-1}), supporting a multilayer/capillary condensation mechanism at higher RH. These thermodynamic trends corroborate the energy-efficiency analysis: the stronger primary binding in MOF-801 favors arid-climate uptake but implies a larger energetic penalty per mole for complete desorption; Al-fumarate's lower Q_{st} facilitates easier regeneration under humid conditions (Makowski, Gryta et al. 2024).

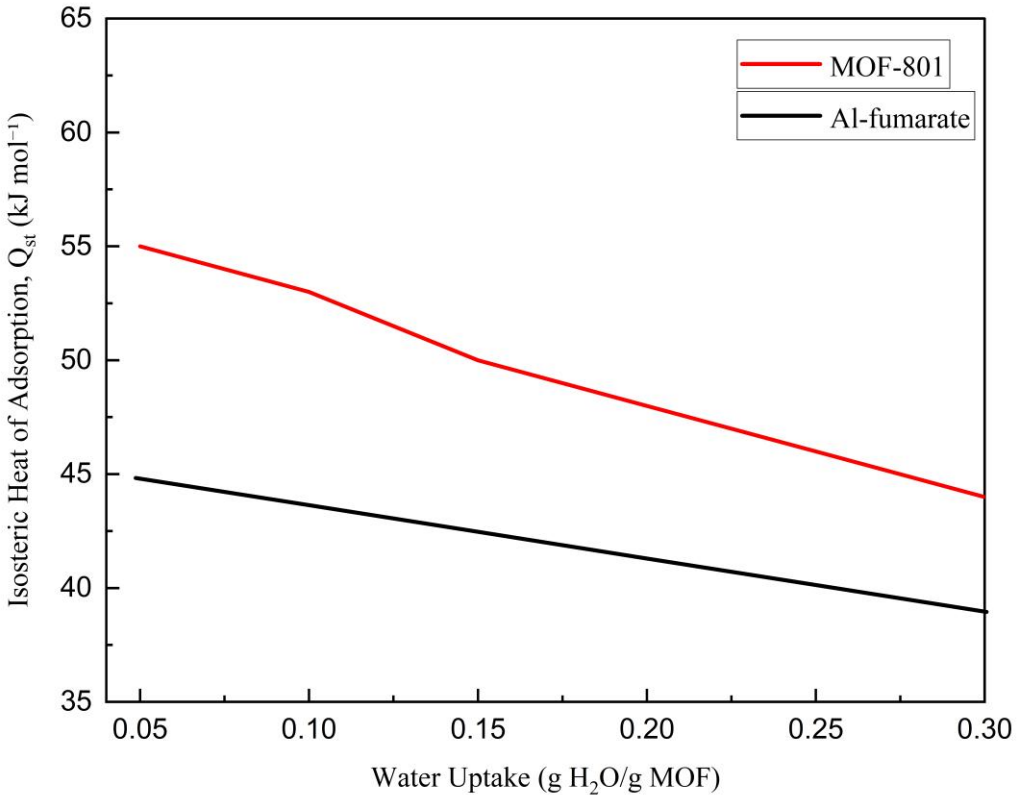
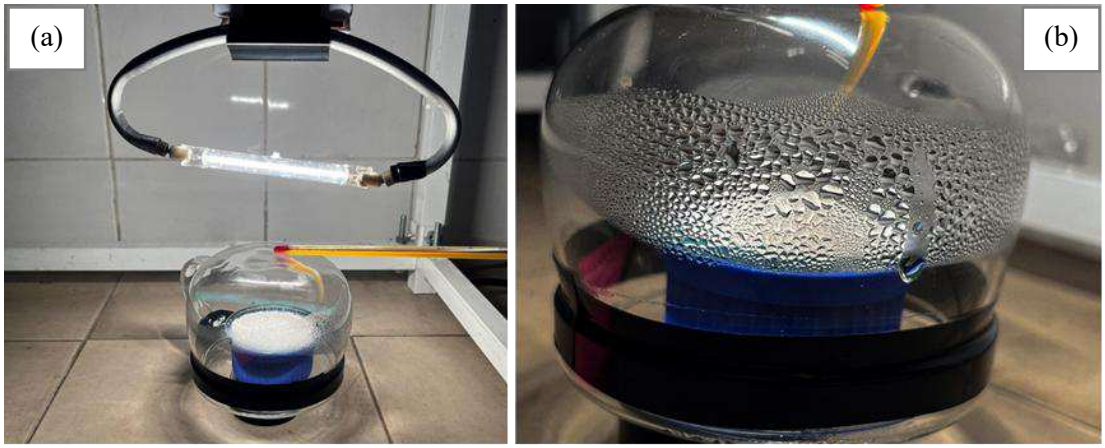


Figure 12. Expected Thermodynamic Trends for Water Adsorption

3.5. Implications for climate-specific AWH design

A separate test assessed the moisture adsorption/desorption capabilities of 2 g MOF-801 and Al-fumarate under realistic environmental conditions. The average adsorption rate of water vapor by the MOF samples was approximately 0.7 g, indicating efficient moisture uptake under ambient conditions. Correspondingly, the average desorption rate measured via condensation inside the Pyrex container was about 0.5 g per cycle, demonstrating effective water release with minimal residual moisture. These values highlight the favorable balance between adsorption capacity and desorption efficiency under low-temperature regeneration (~80°C), supporting the potential of this approach for sustainable atmospheric water harvesting. Desorption was employed using two distinct desorption techniques: convective heating in an oven and radiative heating from a halogen

lamp (simulating solar energy). The data revealed that both MOFs exhibited better moisture removal via radiative heating than oven heating. Oven heating, relying primarily on air circulation and some radiative heat transfer, provides a consistent internal temperature through the even distribution of warmed air. This convective heating process, however, transfers heat less rapidly than direct radiative heating. Conversely, radiative heating directly transfers thermal energy to the MOF sample, creating a high-temperature zone and a substantial temperature gradient between the MOF and the surrounding air. Minor changes also occur within the MOF framework due to light radiation. Upon absorbing this energy, the water molecules could overcome both hydrogen bonding and other van der Waals interactions that retain them inside the MOF structure. These modifications to the framework weaken the interaction between the MOF and water molecules, allowing for desorption.



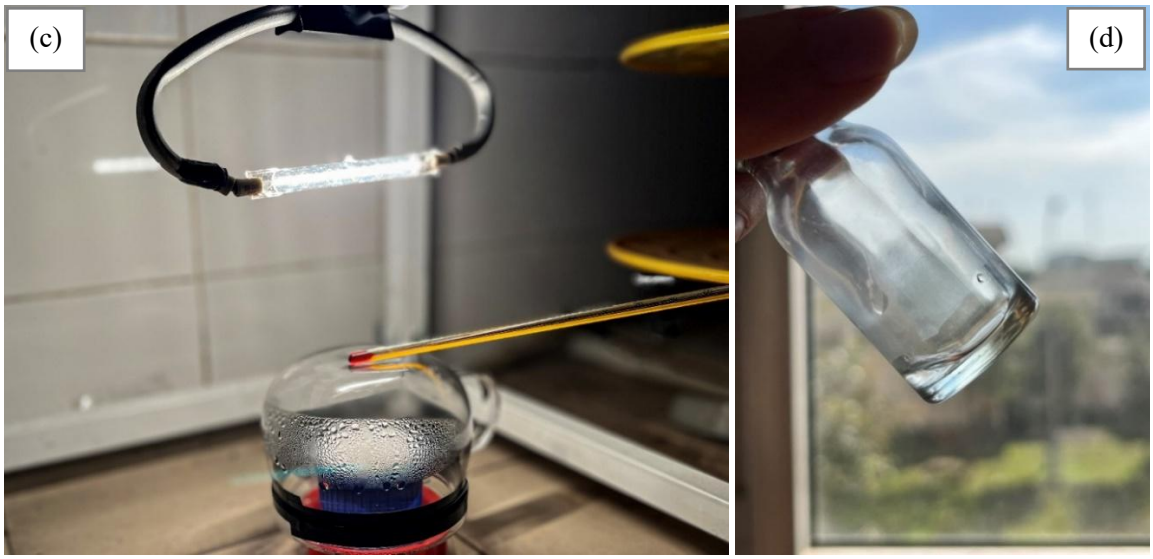


Figure 13. (a) Solar simulated water desorption of MOF-801 and Al-fumarate, (b) The first water drops after 15 minutes, (c) Water desorption after one hour, (d) Collected water from one cycle.

The employed lamp emitted light at specific wavelengths that were potentially resonant with the vibrational modes of water molecules within the MOF, thereby directly increasing their energy and promoting desorption. In contrast, oven heating uniformly warms the entire MOF sample, leading to less efficient energy transfer to water molecules and slower desorption kinetics. Radiative heating raised the MOF temperature above that of the Pyrex container, creating a crucial temperature gradient. When water molecules leave the MOF, they tend to move to lower-temperature regions, such as the Pyrex container. The elevated input energy from the radiation source results in a substantial temperature difference between the MOF and the Pyrex container. This gradient is essential for condensation because water vapor requires a cooler surface. Capillary action within the MOF structure pulls water molecules upward, aided by the adhesive forces that cause water molecules to attract one another—a phenomenon responsible for water's surface tension. The relatively calm surface of the Pyrex container can serve as a condensation site for water vapor released during desorption. The relatively inert Pyrex surface acts as a condensation site, with its likely greater hydrophobicity contrasting with the potentially hydrophilic MOF surface. When water molecules condense on the Pyrex container, cohesive forces form a spherical shape to minimize surface area, resulting in water droplets.

Energy demand during regeneration is a critical parameter for evaluating the practical viability of atmospheric water harvesting (AWH) materials. In this study, both MOF-801 and Al-fumarate demonstrated efficient desorption at relatively low regeneration temperatures (~80 °C),

providing a significant advantage over conventional sorbents, such as zeolites, which typically require temperatures above 150 °C. To quantify this benefit, the specific energy consumption was estimated using equation (3):

$$E = \frac{m_{ads} \times C_p \times \Delta T}{V} \quad (3)$$

Where m_{ads} is the mass of adsorbed water per gram of MOF (g/g), C_p is the specific heat capacity of water, ΔT is the temperature difference between ambient and regeneration temperature, and V is the volume of desorbed water per gram of MOF in liters.

The energy required to regenerate MOF-801 and Al-fumarate was estimated based on an average water uptake of approximately 0.25 g H_2O per gram of MOF per cycle, with regeneration occurring at 80°C. Using the sensible heat formula and accounting for typical heat transfer efficiencies, the specific energy input is calculated to be between 1.2 and 1.5 MJ per liter of water produced. This energy requirement is considerably lower—by approximately 30–40%—than that of conventional zeolite-based sorbents, which often need regeneration temperatures exceeding 150°C, resulting in energy demands above 2 MJ per liter of water. The lower regeneration temperature and associated energy consumption of these MOFs highlight their promise for more sustainable and cost-effective atmospheric water harvesting, especially in energy-limited, arid regions. Such improved efficiency complements their demonstrated water uptake capacities and cycling stability, positioning MOF-801 and Al-fumarate as promising candidates for cost-effective, environmentally friendly water recovery technologies.

4. Conclusion

This study provided a systematic comparison of two zirconium- and aluminum-based MOFs, MOF-801 and Al-fumarate, with emphasis on their potential for atmospheric water harvesting (AWH). The results demonstrate clear contrasts in adsorption mechanisms: MOF-801 favors monolayer uptake at lower humidity, while Al-fumarate benefits from stronger interactions and mesoporous diffusion, leading to higher uptake in more humid, warmer conditions. Laboratory adsorption data confirmed that MOF-801 achieves superior performance at moderate relative humidity, whereas Al-fumarate exhibits greater efficiency at elevated humidity and temperature. This knowledge will be invaluable for optimizing MOF selection based on target humidity

conditions, with MOF-801 exhibiting a higher surface area and water uptake capacity (0.247 $gH_2O/gMOF$ at 40% RH and 20°C) compared to Al-fumarate (water uptake of 0.216 $gH_2O/gMOF$ under similar conditions); however, at 80% humidity and 25°C, Al-fumarate showed superior uptake (0.278 g H_2O/g) versus MOF-801 (0.204 g H_2O/g). Long-term cycling tests across 40 adsorption–desorption cycles revealed excellent durability, with both frameworks maintaining over 95% of their initial capacity. Importantly, regeneration at only 80 °C, particularly when assisted by simulated solar radiation, underscores the low energy demand and practical feasibility of these materials.

Building upon these promising results, several avenues for future research and development emerge:

- Optimization of Synthesis Methods: Further refinement of the microwave-assisted synthesis of Al-fumarate could enhance its surface area and water uptake capacity. Exploring alternative modulators and reaction conditions for MOF-801 synthesis could also optimize its performance.
- Enhancement of Water Uptake: Surface functionalization of both MOFs with highly hydrophilic groups could potentially increase their water uptake capacity at low relative humidity levels. For instance, incorporating amine groups or other polar moieties could enhance water adsorption.
- Development of Composite Materials: Combining MOF-801 and Al-fumarate with other materials, such as polymers or carbon nanotubes, could yield composites with improved mechanical strength, thermal conductivity, and water adsorption properties.
- System-Level Design and Optimization: Developing and optimizing AWH systems incorporating these MOFs to maximize water production and minimize energy consumption is crucial. It includes optimizing the design of adsorption-desorption cycles, heat exchangers, and condensers.
- Field Testing and Scalability Assessment: Conducting extensive field trials in diverse climatic conditions is crucial for evaluating the long-term performance and durability of these MOFs under real-world conditions. It will also inform the design of scalable AWH systems for practical applications.

- Life Cycle Assessment: Conducting a comprehensive life-cycle assessment of AWH systems based on these MOFs is necessary to evaluate their environmental and economic sustainability relative to traditional water sources.

In conclusion, this research offers precious insights into the potential of MOF-801 and Al-fumarate for AWH, laying the groundwork for sustainable solutions to address worldwide water shortage. Future research should focus on optimizing these materials and on developing efficient, scalable AWH systems for practical applications in water-stressed regions.

References

Ahrestani, Z., S. Sadeghzadeh and H. B. M. Emrooz (2023). "An overview of atmospheric water harvesting methods, the inevitable path of the future in water supply." RSC advances **13**(15): 10273–10307.
DOI: 10.1039/d2ra07733g

Asim, N., M. Badiei, M. A. Alghoul, M. Mohammad, N. A. Samsudin, N. Amin and K. Sopian (2021). "Sorbent-based air water-harvesting systems: Progress, limitation, and consideration." Reviews in Environmental Science and Bio/Technology **20**: 257–279.
https://doi.org/10.1007/s11157-020-09558-6

Ejeian, M. and R. Wang (2021). "Adsorption-based atmospheric water harvesting." Joule **5**(7): 1678–1703.
https://doi.org/10.1016/j.joule.2021.04.005

Esmaeilion, F., A. Ahmadi, S. Hoseinzadeh, M. Aliehyaei, S. A. Makkeh and D. Astiaso Garcia (2021). "Renewable energy desalination; a sustainable approach for water scarcity in arid lands." International Journal of Sustainable Engineering **14**(6): 1916–1942.
https://doi.org/10.1080/19397038.2021.1948143

Felix Sahayaraj, A., H. Joy Prabu, J. Maniraj, M. Kannan, M. Bharathi, P. Diwahar and J. Salamon (2023). "Metal–organic frameworks (MOFs): the next generation of materials for catalysis, gas storage, and separation." Journal of Inorganic and Organometallic Polymers and Materials **33**(7): 1757–1781.
https://doi.org/10.1007/s10904-023-02657-1

Feng, A., N. Akther, X. Duan, S. Peng, C. Onggowarsito, S. Mao, Q. Fu and S. D. Kolev (2022). "Recent development of atmospheric water harvesting materials: a review." ACS Materials Au **2**(5): 576–595.
https://doi.org/10.1021/acsmaterialsau.2c00027

Ghasemzadeh, R. (2025). "Water Vapor Adsorption in Microporous and Mesoporous Frameworks for Atmospheric Water Harvesting: Isotherms, Kinetics, and Thermodynamics Insights." Journal of Water Process Engineering.
https://dx.doi.org/10.2139/ssrn.5227316

Ghiasi, B., Z. H. Aslani and T. Alisoltani (2025). "Assessing the feasibility and sustainability of fog water harvesting as an alternative water resource." Scientific Reports **15**(1): 1–10.
https://doi.org/10.1038/s41598-025-03919-3

Hamid, U., P. Vyawahare and C.-C. Chen (2023). "Estimation of isosteric heat of adsorption from generalized Langmuir isotherm." Adsorption **29**(1): 45–64.
https://doi.org/10.1007/s10450-023-00379-x
Hamidifar, H. (2024). Water Crisis in Iran: Causes, Consequences, and Solutions. Water Crises and Sustainable Management in the Global South, Springer**:** 85–109.
https://doi.org/10.1007/978-981-97-4966-9_3
Hanif, S., M. Sultan and T. Miyazaki (2019). "Effect of relative humidity on thermal conductivity of zeolite-based adsorbents: Theory and experiments." Applied Thermal Engineering **150**: 11–18.
https://doi.org/10.1016/j.applthermaleng.2018.12.144
Hanikel, N., M. S. Prévot, F. Fathieh, E. A. Kapustin, H. Lyu, H. Wang, N. J. Diercks, T. G. Glover and O. M. Yaghi (2019). "Rapid Cycling and Exceptional Yield in a Metal-Organic Framework Water Harvester." ACS Cent Sci **5**(10): 1699–1706.
https://doi.org/10.1021/acscentsci.9b00745
Heidari, A., R. Roshandel and V. Vakiloroaya (2019). "An innovative solar assisted desiccant-based evaporative cooling system for co-production of water and cooling in hot and humid climates." Energy Conversion and Management **185**: 396–409.
https://doi.org/10.1016/j.enconman.2019.02.015
Jeremias, F., D. Fröhlich, C. Janiak and S. K. Henninger (2014). "Advancement of sorption-based heat transformation by a metal coating of highly-stable, hydrophilic aluminium fumarate MOF." RSC advances **4**(46): 24073–24082.
DOI: 10.1039/c4ra03794d
Ji, J., R. Wang and L. Li (2007). "New composite adsorbent for solar-driven fresh water production from the atmosphere." Desalination **212**(1-3): 176–182.
https://doi.org/10.1016/j.desal.2006.10.008
Kim, H. (2018). Development of adsorption-based atmospheric water harvesting and thermal energy storage technologies, Massachusetts Institute of Technology.
http://dspace.mit.edu/handle/1721.1/7582
Kim, H., S. Yang, S. R. Rao, S. Narayanan, E. A. Kapustin, H. Furukawa, A. S. Umans, O. M. Yaghi and E. N. Wang (2017). "Water harvesting from air with metal-organic frameworks powered by natural sunlight." Science **356**(6336): 430–434.
DOI: 10.1126/science.aam8743
Kumar, M. and A. Yadav (2015). "Experimental investigation of design parameters of solar glass desiccant box type system for water production from atmospheric air." Journal of Renewable and Sustainable Energy **7**(3).
https://doi.org/10.1063/1.4922142
LaPotin, A., H. Kim, S. R. Rao and E. N. Wang (2019). "Adsorption-Based Atmospheric Water Harvesting: Impact of Material and Component Properties on System-Level Performance." Accounts of Chemical Research **52**(6): 1588–1597.
https://doi.org/10.1021/acs.accounts.9b00062
Logan, M. W., S. Langevin and Z. Xia (2020). "Reversible Atmospheric Water Harvesting Using Metal-Organic Frameworks." Sci Rep **10**(1): 1492.
https://doi.org/10.1038/s41598-020-58405-9
Łuczak, J., M. Kroczewska, M. Baluk, J. Sowik, P. Mazierski and A. Zaleska-Medynska (2023). "Morphology control through the synthesis of metal-organic frameworks." Advances in Colloid and Interface Science **314**: 102864.
https://doi.org/10.1016/j.cis.2023.102864

Makowski, W., P. Gryta, G. Jajko-Liberka, M. Cieślik-Górna and A. Korzeniowska (2024). "Water Sorption Properties and Hydrothermal Stability of Al-Containing Metal–Organic Frameworks CAU-10 and MIL-96 Studied Using Quasi-Equilibrated Thermodesorption." Molecules **29**(23): 5625.
https://doi.org/10.3390/molecules29235625
Meng, Y., Y. Dang and S. L. Suib (2022). "Materials and devices for atmospheric water harvesting." Cell Reports Physical Science **3**(7).
https://doi.org/10.1016/j.xcrp.2022.100976
Mirzavand, M. and R. Bagheri (2020). "The water crisis in Iran: Development or destruction?" World Water Policy **6**(1): 89–97.
https://doi.org/10.1002/wwp2.12023
Mulchandani, A., S. Malinda, J. Edberg and P. Westerhoff (2020). "Sunlight-driven atmospheric water capture capacity is enhanced by nano-enabled photothermal desiccants." Environmental Science: Nano **7**(9): 2584–2594.
https://doi.org/10.1039/D0EN00463D
Pimentel, D., B. Berger, D. Filiberto, M. Newton, B. Wolfe, E. Karabinakis, S. Clark, E. Poon, E. Abbett and S. Nandagopal (2004). "Water resources: agricultural and environmental issues." BioScience **54**(10): 909–918.
https://doi.org/10.1641/0006-3568(2004)054[0909:WRAAEI]2.0.CO;2
Rieth, A. J., S. Yang, E. N. Wang and M. Dincă (2017). "Record atmospheric fresh water capture and heat transfer with a material operating at the water uptake reversibility limit." ACS central science **3**(6): 668–672.
https://doi.org/10.1021/acscentsci.7b00186
Rouhani, F. and M. Ghiasvand (2024). "Pore engineering of a Quasi-MOF-801 with unsaturated metal site and modulate porosity for selective and effective phosphate uptake." Microporous and Mesoporous Materials **366**: 112941.
https://doi.org/10.1016/j.micromeso.2023.112941
Roy, S., S. Laha and T. K. Maji (2019). Potential of hydrophobic metal-organic framework-based materials for environmental applications. Metal-Organic Frameworks (MOFs) for Environmental Applications, Elsevier**:** 319–354.
https://doi.org/10.1016/B978-0-12-814633-0.00010-7
Saidi, M., P. H. Ho, P. Yadav, F. Salles, C. Charnay, L. Girard, L. Boukli-Hacene and P. Trens (2021). "Zirconium-based metal organic frameworks for the capture of carbon dioxide and ethanol vapour. A comparative study." Molecules **26**(24): 7620.
https://doi.org/10.3390/molecules26247620
Sultan, M., M. Bilal, T. Miyazaki, U. Sajjad and F. Ahmad (2021). "Adsorption-based atmospheric water harvesting: technology fundamentals and energy-efficient adsorbents." Technology in Agriculture; Ahmad, F., Sultan, M., Eds: 369.
DOI: 10.5772/intechopen.97301
Tashtoush, B. and A. Alshoubaki (2023). "Atmospheric water harvesting: A review of techniques, performance, renewable energy solutions, and feasibility." Energy **280**: 128186.
https://doi.org/10.1016/j.energy.2023.128186
Tatlier, M., G. Munz and S. K. Henninger (2018). "Relation of water adsorption capacities of zeolites with their structural properties." Microporous and Mesoporous Materials **264**: 70–75.
https://doi.org/10.1016/j.micromeso.2017.12.031

Wang, M., E. Liu, T. Jin, S.-u. Zafar, X. Mei, M.-L. Fauconnier and C. De Clerck (2024). "Towards a better understanding of atmospheric water harvesting (AWH) technology." Water Research **250**: 121052.
https://doi.org/10.1016/j.watres.2023.121052
Wei, X., W. Wang, J. Xiao, L. Zhang, H. Chen and J. Ding (2013). "Hierarchically porous aluminosilicates as the water vapor adsorbents for dehumidification." Chemical engineering journal **228**: 1133–1139.
https://doi.org/10.1016/j.cej.2013.05.062
Xu, W. and O. M. Yaghi (2020). "Metal–organic frameworks for water harvesting from air, anywhere, anytime." ACS central science **6**(8): 1348–1354.
https://dx.doi.org/10.1021/acscentsci.0c00678
Yang, C., H. Wu, J. Yun, J. Jin, H. Meng, J. Caro and J. Mi (2023). "Engineering of Defective MOF-801 Nanostructures within Macroporous Spheres for Highly Efficient and Stable Water Harvesting." Advanced materials (Deerfield Beach, Fla.) **35**: e2210235.
https://doi.org/10.1002/adma.202210235
Yilmaz, G., F. Meng, W. Lu, J. Abed, C. Peh, M. Gao, E. Sargent and G. Ho (2020). "Autonomous atmospheric water seeping MOF matrix." Science advances **6**(42): eabc8605.
DOI: 10.1126/sciadv.abc8605
Zahn, G. (2015). "Synthesis and characterisation of Zr-fumarate MOF: a promising candidate for biomedical applications."
DOI: 10.1126/sciadv.abc8605
Zeng, W., T. You and W. Wu (2024). "Passive atmospheric water harvesting: Materials, devices, and perspectives." Nano Energy **125**: 109572.
https://doi.org/10.1016/j.nanoen.2024.109572
Zhang, H., J. Nai, L. Yu and X. W. D. Lou (2017). "Metal-organic-framework-based materials as platforms for renewable energy and environmental applications." Joule **1**(1): 77–107.
https://doi.org/10.1016/j.joule.2017.08.008
Zhao, H., Q. Li, Z. Wang, T. Wu and M. Zhang (2020). "Synthesis of MIL-101 (Cr) and its water adsorption performance." Microporous and Mesoporous Materials **297**: 110044.

https://doi.org/10.1016/j.micromeso.2020.110044

Acknowledgements

The authors would like to thank the staff of the Chemical Engineering Laboratory, University of Guilan, for technical assistance and laboratory support.

Funding

This research received no specific grant from any funding agency in the public, commercial, or not-for-profit sectors.

Authors' Contributions

Ayda Naghavi: performed the experiments, data collection, derived the models and analyzed the data. Fereshteh Raouf: supervision, project management, designed the experiments and final editing of the

manuscript. Reza Ghasemzadeh: analysis of existing literature, and writing original draft, visualization of results.

Ethical Approval

This study does not involve human subjects or animals.

Consent to Participate

This is not applicable.

Consent to Publish

The authors consent to publication of this manuscript.

Competing Interests

The authors declare no competing interests.

Data Availability Statement

All data and materials referenced in this article are generated in our lab and were used in original paper.